UNIVERSIDADE FEDERAL DO RIO GRANDE DO SUL
INSTITUTO DE FÍSICA

Programa de Pós-Graduação em Física

Bruna Mezzari Carlos

Establishing limits for monopole production in pp collisions

Porto Alegre, Brasil
30 de Dezembro de 2020

Bruna Mezzari Carlos

Establishing limits for monopole production in pp collisions

Estabelecendo Limites para a produção de monopolos em colisões pp

Master's dissertation presented at the Instituto de Física da Universidade Federal do Rio Grande do Sul as a partial requisite for the degree of Master of Science in Theoretical Physics.

Supervisor: Maria Beatriz Gay Ducati

Porto Alegre, Brasil
30 de Dezembro de 2020

Agradecimentos

Gostaria de agradecer à minha orientadora, Maria Beatriz Gay, por todo o apoio e orientação durante minha graduação e mestrado.

Á minha mãe, minha irmã e ao Henrique por todo o amor e suporte durante essa jornada.

Abstract

The magnetic monopole-antimonopole pair production by photon fusion and Drell Yan and monopolium production by photon fusion processes are calculated in proton-proton collisions. Two different coupling models are used, the usual velocity-dependent and the velocity dependent with a magnetic moment parameter. The mass range used for the monopole is based on the last results of ATLAS and the MoEDAL experiment that set a minimal mass of around 2 TeV for the spin 1/2 monopole. The cross sections are calculated with the center of mass energies of LHC, for its successor, the HE-LHC and the future collider FCC. In a complement to the cross sections, the energy distributions that can improve the chances of detection are analyzed.

Resumo

A produção de par monopolo-antimonopolo magnético via fusão de fótons e Drell Yan e a produção de monopolium por fusão de fótons, são calculados para colisões próton-próton. Dois diferentes modelos de acoplamento são usados, um dependendo da velocidade, e um segundo em função da velocidade e momento magnético. A escala de massa utilizada para o monopolo é baseada nos últimos resultados dos experimentos ATLAS e MoEDAL no LHC, que estimaram um limite mínimo de massa em cerca de 2 TeV para um monopolo de spin 1/2. As seções de choque foram calculadas para energias de colisão do LHC, e também para os futuros experimentos HE-LHC e FCC. Em complemento às seções de choque, também são estudadas distribuições de energia, que podem aumentar a chance de detecção dessa nova partícula.

List of Figures

Contents

Introduction

Since one of the first theories about magnetic monopoles, proposed by Dirac in his two papers [1] and [2], a number of experiments[3][4] were not able to prove its existence. Dirac's monopole is a point-like particle responsible for giving symmetry between the electric and magnetic interactions and explaining the electric charge quantization, by the Dirac quantization condition (DQC)

$$ge = 4\pi\frac{n}{2}, \tag{1}$$

with g and e the magnetic monopole and electron charges, respectively, and n an integer. New models for this unknown particle were proposed later on, like the dyon, a particle with both electric and magnetic charges theorized by Schwinger [5], and the monopoles in electroweak[6] and unification theories [7][8][9][10][11]. While in Dirac's model the coupling force between a monopole-antimonopole pair is about 10^3 times stronger than the one between an electron and a positron, the principal issue in unification theories is that the expected mass for the monopole is around 10^{15} Gev. A possible explanation for the lack of experimental evidence of monopoles was first given in [12], where it was assumed that due to the strong magnetic coupling the magnetic poles would always be in a bound state, called monopolium. In the same paper it is also studied the hypothesis of relic monopoles, produced in the early universe, that could still be detected nowadays in a bounded form. Also, the products from the decay of monopoles produced in the early universe could still be observed in measures of the cosmic microwave background anisotropy and primordial gravitational waves[13].

In the scenario where no formal theory to treat magnetic monopole interactions is fully developed, some effective couplings have been proposed. The minimalistic model treats the moving monopole as an electric charge, so that it couples to the photon just like the electron. This idea was used to determine the first limits on Dirac's monopole mass [14][3] and has been used since then in many theoretical works [15][16][17] and in the current experimental search for monopoles [18][19][20]. A more recent work [21] proposed the addition of a magnetic moment term to the usual velocity-dependent coupling. With this new parameter, the limits where perturbation methods can be used are increased.

The pair production of monopoles (a monopole and an antimonopole) will be studied by two processes in leading order: photon fusion and Drell Yan (see Figures 3.2 and 3.6). The fusion of two photons to form a pair of leptons or charged scalar particles has been widely covered [22] and used to investigate the Higgs boson production[23][24] and particles beyond the Standard Model[25]. Also, due to the great magnetic charge, the photon fusion cross sections are expected to be greatly enhanced. In collisions involving protons, the Drell Yan mechanism[26] can also be

used to investigate such particles, as it has been proved[27] that for lepton and Higgs production the cross sections for Drell Yan are $\sim 10^2$ times larger than those for photon fusion. An opposite behavior occurs when one uses the velocity dependent magnetic coupling[15], which makes the photon fusion process a relevant candidate to consider for monopole observation. The two models of coupling cited in the paragraph above will be used.

The current experiments dedicated to the search of magnetic monopoles in proton-proton collisions are in the MoEDAL[18] experiment and the ATLAS[28] detectors in the LHC. The last results of MoEDAL[19] set a minimum value for the monopole mass $m \leq 1320$ GeV considering only Drell Yan and $m \leq 2420$ GeV considering both Drell Yan and photon fusion production, for a spin 1/2 monopole with unitary magnetic charge ($n = 1$ in the DQC). The last ATLAS results[20] set a lower bound of 2370 GeV, considering only Drell Yan production for the same type of monopole. These results were obtained by the analysis of data from 2015 to 2017, when the LHC was operating with 13 TeV of center of mass energy for pp collisions. Even with the high limits above it is still possible to produce and detect monopoles in the LHC, especially after the start of RUN 3 scheduled for 2021 and the HL-LHC[29] in 2026. Beyond the LHC, we will also consider the energies of the HE-LHC[30], the successor of LHC, and the FCC[31] colliders.

This work is organized as follows: in Chapter 1 Dirac's theory for magnetic monopoles is introduced and some comments on the classic theory with monopoles are made; in Chapter 2 some basic concepts of quantum field theory are introduced, and then the two coupling models are presented; in Chapter 3 the two processes for monopole and monopolium production are presented and in Chapter 4 how they are inserted in pp collisions, together with a photon flux model for the proton and comments on the magnetic monopole current experiments. In Chapter 5 the results and conclusions are presented.

A version of this work in article form can be seen in [32] and [33].

Chapter 1

Dirac Magnetic Monopoles

1.1 Dirac Quantization Condition

In the paper of 1931 [1], Dirac showed by simple arguments that magnetic monopoles are allowed in quantum mechanics and also explain charge quantization. To do so, he followed the simple logical arguments:

First, one writes a general wave function with undetermined phase in the following way

$$\psi = \psi_1 \mathrm{e}^{i\beta}, \tag{1.1}$$

where ψ_1 has definite phases for each point and β is a real number with derivatives

$$\nabla\beta \equiv \vec{\kappa}, \quad \frac{\partial\beta}{\partial t} \equiv \kappa_0. \tag{1.2}$$

Now, if ψ satisfies the free particle wave equation

$$\frac{(-ih)^2}{2m}\nabla^2\psi = ih\frac{\partial\psi}{\partial t} \tag{1.3}$$

ψ_1 will satisfy

$$\left(-ih\nabla + h\vec{\kappa}\right)^2 \psi_1 = \left(ih\frac{\partial}{\partial t} - h\kappa_0\right)\psi_1, \tag{1.4}$$

which corresponds to a displacement in the momentum $\vec{p}$ by $\vec{p}+h\vec{\kappa}$ and in the energy E by $E - h\kappa_0$. However, equation (1.4) is the usual wave equation for a particle with charge $-e$ in an electromagnetic field with potential

$$\vec{A} = \frac{hc}{e}\vec{\kappa}, \quad A_0 = -\frac{h}{e}\kappa_0, \tag{1.5}$$

and one can write the electric and magnetic fields as

$$\nabla \times \vec{\kappa} = \frac{e}{hc}\vec{H}, \quad \nabla\kappa_0 - \frac{\partial\vec{\kappa}}{\partial t} = \frac{e}{h}\vec{E}. \tag{1.6}$$

The change in phase around a closed curve defining a surface ϵ in space will be

$$\int_{\delta\epsilon} \vec{\kappa}\cdot d\vec{r} = \int_{\epsilon} \nabla\times\vec{\kappa}\cdot d\vec{\epsilon}. \tag{1.7}$$

Taking into account that a phase is always undetermined by a multiple of 2π, if the change around a closed curve has to be the same for all wave functions, then

equation (1.7) has to be modified. Assuming the continuity of the wave function and taking a very small closed curve, the change in phase must be very small so that it cannot differ from multiples of 2π for different wave functions. However, when the wave function vanishes its phase is not relevant anymore. In a complex space the points where the wave function vanishes define a line, which is called nodal line. If a nodal line passes through a small closed curve, the change in phase does not need to be small anymore, and it will be close to $2\pi n$, with n being a integer (positive or negative) that characterizes the curve. The difference between the change in phase of the wave function with a nodal line passing through a small curve and the nearest $2\pi n$ must be the same for all wave functions, and (1.7) becomes

$$2\pi \sum n + \frac{e}{hc} \int_{\epsilon} \vec{H} \cdot d\vec{\epsilon}, \tag{1.8}$$

where the sum is over all nodal lines that pass through the curve. For a closed curve, equation (1.8) must vanish and the sum over all the nodal lines will be proportional to the magnetic flux. If the sum $\sum n$ does not vanish, then there must be some nodal lines with end points on the surface of the closed curve, for the ones that pass through must have a positive and a negative contribution that cancel each other. Around one of these points, the magnetic flux will be

$$\frac{2\pi hc}{e} n \equiv 4\pi g, \tag{1.9}$$

and the end point of the nodal line represents a singularity in the electromagnetic field, a magnetic pole with magnetic charge g. Then, the relation between the electric and magnetic charge

$$ge = hc\frac{n}{2}, \tag{1.10}$$

or in SI natural units ($\hbar = c = 1$)

$$ge = 2\pi\frac{n}{2}, \tag{1.11}$$

explains the charge quantization. Taking $n = 1$, Dirac also defined the unitary magnetic charge as function of the elementary electric charge e_o

$$g_o \approx 68,5 e_o. \tag{1.12}$$

1.2 Classic Scenario

1.2.1 Electric and Magnetic Charge Interaction

If one considers the magnetic monopole to be a point-like particle with magnetic charge g in the classic framework, a simple assumption of symmetry with the electron would give a magnetic field

$$\mathbf{B} = g\frac{\mathbf{r}}{r^3}, \tag{1.13}$$

where $r = |\mathbf{r}|$ and the monopole is at the origin of the reference frame. The respective equation of motion of an electrically charged particle e in the position $\mathbf{r}$ with velocity $\mathbf{v}$ will be

$$m\frac{d^2\mathbf{r}}{dt^2} = e[\mathbf{v} \times \mathbf{B}] = \frac{eg}{r^3}\left[\frac{d\mathbf{r}}{dt} \times \mathbf{r}\right]. \tag{1.14}$$

One of the constants of motion can be obtained with the scalar multiplication of (1.14) by $\mathbf{v}$

$$m\mathbf{v}\cdot\frac{d^2\mathbf{r}}{dt^2}=\frac{m}{2}\frac{dv^2}{dt}=0,$$

which gives the conservation of kinetic energy

$$T=\frac{mv^2}{2}=\text{constant}. \tag{1.15}$$

The second constant of motion can be obtained by making the scalar product of (1.14) with $\mathbf{r}$

$$m\mathbf{r}\cdot\frac{d^2\mathbf{r}}{dt^2}=m\left[\frac{1}{2}\frac{d^2r^2}{dt^2}-v^2\right]=0,$$

and considering the first constant (1.15)

$$r=\sqrt{v^2t^2+b^2}, \tag{1.16}$$

with b the initial position of the electric particle. Equation (1.16) implies that there is no closed orbit in the system considered, and the charged particle will be carried from a initial point $\mathbf{b}$ to infinity.

1.2.2 Vector Potential

Now, to describe the interaction between a magnetic and an electric charge, it is necessary to generalize the standard Lagrangian for a charge in an external field

$$L=\frac{m}{2}\left(\frac{d\mathbf{r}}{dt}\right)^2+e\frac{d\mathbf{r}}{dt}\cdot\mathbf{A}, \tag{1.17}$$

where $\mathbf{A}$ is the vector potential. According to (1.13), the vector potential should satisfy

$$\mathbf{B}=g\frac{\mathbf{r}}{r^3}=\nabla\times\mathbf{A}, \tag{1.18}$$

but this generates a contradiction when the magnetic charge is the generator of the field

$$\nabla\cdot\mathbf{B}=4\pi g\delta^{(3)}(\mathbf{r}), \tag{1.19}$$

for (1.18) requires that $\nabla\cdot\mathbf{B}=0$. To try to solve this problem, one could use the radial symmetry of (1.13) and write the potential in the form [34]

$$\mathbf{A}(\mathbf{r})=A(\theta)\nabla\phi, \tag{1.20}$$

where ϕ and θ are the azimuthal and polar angles, respectively, in spherical coordinates. Taking $A(\theta)=-g(1+\cos\theta)$ with

$$\nabla\phi=\left(-\frac{\sin\phi}{r\sin\theta},\ \frac{\cos\phi}{r\sin\theta},\ 0\right), \tag{1.21}$$

the potential will be

$$\mathbf{A}(\mathbf{r})=\left(g\frac{1+\cos\theta}{r\sin\theta}\sin\phi,\ -g\frac{1+\cos\theta}{r\sin\theta}\cos\phi,\ 0\right)=\frac{g}{r}\frac{\mathbf{r}\times\hat{\mathbf{k}}}{r-\mathbf{r}\cdot\hat{\mathbf{k}}}, \tag{1.22}$$

where $\hat{\mathbf{k}} = (0, 0, 1)$, and one can easily see that with this choice of potential equation (1.18) is satisfied. However, in (1.22) $\mathbf{A}$ is singular at the line $\theta = 0$ and a regularized potential can be defined[35]

$$\mathbf{A}_R(\mathbf{r}, \epsilon) = \frac{g}{R} \frac{\mathbf{r} \times \hat{\mathbf{k}}}{R - \mathbf{r} \cdot \hat{\mathbf{k}}}, \tag{1.23}$$

where $R = \sqrt{r^2 + \epsilon^2}$, and the regularized magnetic field will be

$$\mathbf{B}_R(\mathbf{r}, \epsilon) = g\frac{\mathbf{r}}{R^3} - g\epsilon^2 \left(\frac{\hat{\mathbf{k}}}{R^3[R - \mathbf{r} \cdot \hat{\mathbf{k}}]} + \frac{\hat{\mathbf{k}}}{R^2[R - \mathbf{r} \cdot \hat{\mathbf{k}}]^2} \right). \tag{1.24}$$

Taking the limit $\epsilon^2 \to 0$,

$$\mathbf{B}_R(\mathbf{r}, \epsilon) \sim g\frac{\mathbf{r}}{r^3} - 2g\epsilon^2 \hat{\mathbf{k}}\theta(z) \left(\frac{1}{r^2(x^2 + y^2 + \epsilon^2)} + \frac{2}{(x^2 + y^2 + \epsilon^2)^2} \right). \tag{1.25}$$

Because of the $\theta(z)$, the singular terms will be non-zero only in the $z > 0$ hemisphere. Taking the magnetic flux of an element of surface around the z axis, the only contribution comes from the second term in parenthesis, and the magnetic field can be written as

$$\mathbf{B}_R(\mathbf{r}) = \mathbf{B}_g(\mathbf{r}) + \mathbf{B}_{sing}(\mathbf{r}) = g\frac{\mathbf{r}}{r^3} - 4\pi g\theta(z)\delta(x)\delta(y)\hat{\mathbf{k}}. \tag{1.26}$$

Now,

$$\nabla \cdot \mathbf{B} = \nabla \cdot \mathbf{B}_g + \nabla \cdot \mathbf{B}_{sing} = 4\pi g\delta^{(3)}(r) - 4\pi g\delta^{(3)}(r) = 0, \tag{1.27}$$

and $\mathbf{B}$ can be defined as the curl of $\mathbf{A}$. The singular term of the magnetic field recovers the concept of the Dirac nodal line, that goes from infinity to the pole, as depicted in Figure 1.1.

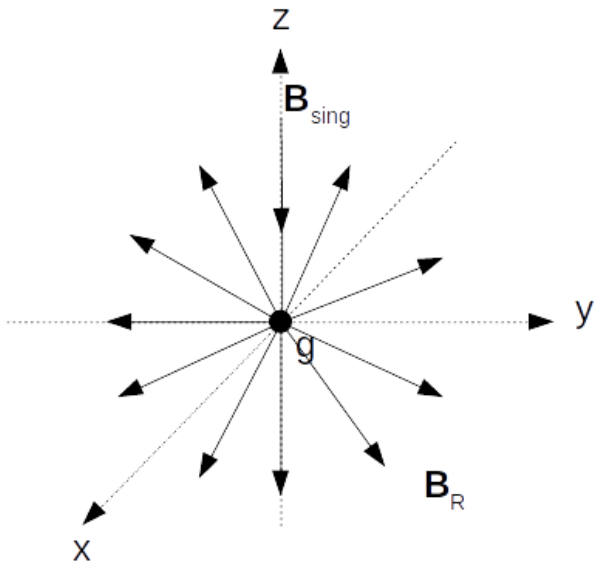

Figure 1.1: Singular and radial magnetic fields of a magnetic charge.

1.2.3 Gauge Transformations

The gauge transformations for the vector potential in the usual electrodynamics can be written in the form

$$\mathbf{A} \to \mathbf{A}' = \mathbf{A} + \nabla\lambda(\mathbf{r}), \tag{1.28}$$

with $\lambda(\mathbf{r})$ an arbitrary function. The singularity in (1.22) leads to think that nodal lines are not observable structures and consequently a change in their positions would not modify the properties of the system. To prove this, it is necessary to first analyze the variation in the magnetic flux after the transformation (1.28)

$$\Delta\Phi = \int (\mathbf{B}' - \mathbf{B}) \cdot \hat{\mathbf{n}}_S \, d^2S = \int [\nabla \times \nabla\lambda(\mathbf{r})] \cdot \hat{\mathbf{n}}_S \, d^2S = \oint \nabla\lambda(\mathbf{r}) \cdot \, d\mathbf{l}. \tag{1.29}$$

Choosing λ to be symmetric over the polar angle $\lambda(\mathbf{r}) = 2g\phi = 2g \arctan y/x$, the new potential is

$$\mathbf{A}'(\mathbf{r}) = \frac{g}{r} \frac{\mathbf{r} \times \hat{\mathbf{k}}}{r - \mathbf{r} \cdot \hat{\mathbf{k}}} + \frac{2g}{r \sin\theta}(-\sin\phi\,\hat{\mathbf{i}} + \cos\phi\,\hat{\mathbf{j}}) = \frac{g}{r}\frac{1 - \cos\theta}{\sin\theta}\hat{\mathbf{e}}_\phi, \tag{1.30}$$

with $\hat{\mathbf{i}}$, $\hat{\mathbf{j}}$ and $\hat{\mathbf{e}}_\phi$ the unitary vectors in the directions x, y and ϕ, respectively. The potential is now singular at the semi infinite axis $\theta = \pi$, and the variation in the magnetic flux along the z axis, $\Delta\Phi = 4\pi g$, represents a nodal line that comes from the negative infinity of the z axis to the pole. That choice of gauge results in a π rotation of the string, which proves that the string and its field are not physical.

Other types of gauge have been studied and give interesting results, such as the one proposed by Schwinger[36] $\lambda(\mathbf{r}) = g\phi$, that generates the potential

$$\mathbf{A}^{Sch}(\mathbf{r}) = -\frac{g}{r}\frac{\sin\theta}{\cos\theta}\hat{\mathbf{e}}_\phi. \tag{1.31}$$

The Schwinger potential is singular over all the z axis, representing an infinite nodal line that pass through the magnetic charge.

It is also worth to note that the new potential (1.22) is no longer symmetric under parity transformations,

$$\mathbf{A}(-\mathbf{r}) = -\frac{g}{r}\frac{\mathbf{r} \times \hat{\mathbf{k}}}{r + \mathbf{r} \cdot \hat{\mathbf{k}}} \neq \pm\mathbf{A}(\mathbf{r}), \tag{1.32}$$

since $\hat{\mathbf{k}}$ is fixed. However, the transformed potential (1.30)

$$\mathbf{A}'(-\mathbf{r}) = \frac{g}{r}\frac{1 - \cos\theta}{\sin\theta} = \mathbf{A}'(\mathbf{r}) \tag{1.33}$$

behaves as a pseudo-vector, meaning that the existence of a magnetic pole could affect the parity violation[37][38].

1.3 Dirac's Theory

In his second paper about magnetic monopoles [2], Dirac properly introduced the monopoles in the electrodynamics formulation. The usual Maxwell's equations, in natural units and metric $(1, -1, -1, -1)$ can be written in the covariant form:

$$\frac{\partial F_{\mu\nu}}{\partial x_\nu} = 4\pi j_\mu, \quad \frac{\partial \tilde{F}_{\mu\nu}}{\partial x_\nu} = 0 \quad (\tilde{F}_{\mu\nu} = \epsilon^{\alpha\beta\mu\nu} F_{\alpha\beta}/2), \tag{1.34}$$

with j_μ the electric current density and $F_{\mu\nu}$ the electromagnetic tensor

$$F_{\mu\nu} = \begin{pmatrix} 0 & E_x & E_y & E_z \\ -E_x & 0 & -B_z & B_y \\ -E_y & B_z & 0 & -B_x \\ -E_z & -B_y & B_x & 0 \end{pmatrix}. \tag{1.35}$$

With the presence of monopoles in the theory, a magnetic current density k_μ can be added to (1.34) so that both equations are symmetric

$$\frac{\partial F_{\mu\nu}}{\partial x_\nu} = 4\pi j_\mu, \quad \frac{\partial \tilde{F}_{\mu\nu}}{\partial x_\nu} = 4\pi k_\mu, \tag{1.36}$$

where the currents are defined as

$$j_\mu(k_\mu) = \sum_{e(g)} e(g) \int \delta^4(x - z) \frac{dz_\mu}{ds}\, ds, \tag{1.37}$$

with z_μ the position of the particle, x_μ the point of observation and s the invariant Lorentz length $ds^2 = \eta_{\mu\nu} dx^\mu dx^\nu$.

In the traditional theory, $F_{\mu\nu}$ is written in terms of the electromagnetic potential

$$F_{\mu\nu} = \frac{\partial A_\nu}{\partial x^\mu} - \frac{\partial A_\mu}{\partial x^\nu}, \tag{1.38}$$

but to match with (1.36), a new potential has to be introduced, such as

$$F_{\mu\nu} = \frac{\partial A_\nu}{\partial x^\mu} - \frac{\partial A_\mu}{\partial x^\nu} + 4\pi \sum_g \tilde{G}^{\mu\nu}. \tag{1.39}$$

The proposition of Dirac in [2] is that equation (1.38) must fail in one point on every surface that contains a monopole, so that the new potential $G_{\mu\nu}$ is defined in a way to cover these points

$$\partial G_{\mu\nu}/\partial x_\nu = g \int \frac{dz_\mu}{ds} \delta^{(4)}(x - z)\, ds, \tag{1.40}$$

and to recover the right equation in (1.36). All the points in which equation (1.38) fails will form strings (in space-time) that will start in each monopole and extend to infinite, resembling the concept of nodal lines in [1]. These lines were also called strings and can be parameterized by

$$y_\mu(\tau, \sigma) = z_\mu(\tau) + \eta_\mu(\tau, \sigma), \tag{1.41}$$

with τ and σ being a time and a spatial parameters, respectively, and $y_\mu(\tau = 0, \sigma) = z_\mu(s)$ the initial condition, so that the line starts at the pole. The new potential can then be written in terms of the string coordinates

$$G_{\mu\nu}(z, y) = g \int \int \left(\frac{dy_\mu}{d\tau} \frac{dy_\nu}{d\sigma} - \frac{dy_\mu}{d\sigma} \frac{dy_\nu}{d\tau} \right) \delta(z - y(\tau, \sigma))\, d\tau d\sigma. \tag{1.42}$$

With the field tensor established, the action functional will be given by

$$S = -\frac{1}{4} \int F_{\mu\nu} F^{\mu\nu}\, d^4x + \int A^\mu j_\mu^{(e)}\, d^4x + m_e \int ds^{(e)} + m_g \int ds^{(g)}. \tag{1.43}$$

Taking the variation with respect to the potential A_μ gives the first equation of (1.36), while the second one is given as a restriction for $G_{\mu\nu}$ (1.40). The variation of (1.43) with respect to the magnetic charge trajectories gives

$$m_g \frac{d^2 z_\mu}{ds^2} = g\tilde{F}_{\mu\nu}\frac{dz^\nu}{ds}, \tag{1.44}$$

as expected. The variation with respect to the electric charge gives

$$m_e \frac{d^2 z_\mu}{ds^2} = e\left(\frac{\partial A_\nu}{\partial x^\mu} - \frac{\partial A_\mu}{\partial x^\mu}\right)_{x=z} \frac{dz^\nu}{ds}, \tag{1.45}$$

which does not correspond to the usual equation of motion

$$m_e \frac{d^2 z_\mu}{ds^2} = eF_{\mu\nu}\frac{dz^\nu}{ds},$$

for $F_{\mu\nu}$ is now modified (1.39). To solve this problem, Dirac proposed[2] the restriction that no electric charge should pass through a string, $z_\mu^{(e)}(\tau) \neq y_\mu(\tau,\sigma)$. This condition can also be derived taking the variation with respect to the string variable n_μ

$$\frac{\partial F_{\mu\nu}}{\partial y_\mu} = 0, \tag{1.46}$$

and using that $\partial_\mu F_{\mu\nu} = j_\mu^{(e)}(z_\mu)$, one has $j^{(e)}(y_\mu) = 0$.

The theory developed by Dirac may seem simple, but is far from being self-contained. Some fundamental topics for the development of the theory are still not completely understood, such as

- mass and spin of the monopole (not specified in the theory);
- interaction of the monopole with its own field;
- the magnetic moment of the monopole;
- the non perturbative coupling of the monopoles.

For the last two items, effective lagrangians have been built to derive Feynman rules and cross sections for photon fusion and Drell Yan processes, to be shown in Chapter 2.

1.4 Dual Invariance of the Electromagnetic Field

The free Maxwell's equations

$$\begin{aligned} \nabla\cdot\mathbf{E} = 0, \quad \nabla\cdot\mathbf{B} = 0, \\ \nabla\times\mathbf{E} + \frac{\partial\mathbf{B}}{\partial t} = 0, \quad \nabla\times\mathbf{B} - \frac{\partial\mathbf{E}}{\partial t} = 0 \end{aligned} \tag{1.47}$$

exhibit a clear invariance under the transformations

$$\begin{aligned} \mathbf{E} &\to \mathbf{E}\cos\theta - \mathbf{B}\sin\theta \\ \mathbf{B} &\to \mathbf{E}\sin\theta + \mathbf{B}\cos\theta. \end{aligned} \tag{1.48}$$

In a compact form, the transformations can be written as

$$\mathbf{E} + i\mathbf{B} \rightarrow \mathrm{e}^{i\theta}(\mathbf{E} + i\mathbf{B}). \tag{1.49}$$

This symmetry is also present when writing the free equations (1.36) in the covariant notation

$$\partial_\mu F^{\mu\nu} = 0, \quad \partial_\mu \tilde{F}^{\mu\nu} = 0, \tag{1.50}$$

and the transformation now reads as

$$\begin{aligned} F^{\mu\nu} &\rightarrow F^{\mu\nu}\cos\theta - \tilde{F}^{\mu\nu}\sin\theta, \\ \tilde{F}^{\mu\nu} &\rightarrow F^{\mu\nu}\sin\theta + \tilde{F}^{\mu\nu}\cos\theta. \end{aligned} \tag{1.51}$$

The free Lagrangian will transform as

$$\begin{aligned} \mathscr{L}_o = -\frac{1}{4}F_{\mu\nu}F^{\mu\nu} \rightarrow \mathscr{L}_o &= -\frac{1}{4}F_{\mu\nu}F^{\mu\nu}\cos 2\theta - \frac{1}{4}F_{\mu\nu}\tilde{F}^{\mu\nu}\sin 2\theta \\ &= -\frac{1}{2}\cos 2\theta(\mathbf{E}^2 - \mathbf{B}^2) - \frac{1}{2}\sin 2\theta(\mathbf{E}\cdot\mathbf{B}). \end{aligned} \tag{1.52}$$

The extra term in the transformed Lagrangian

$$F_{\mu\nu}\tilde{F}^{\mu\nu} = 2\partial_\mu(A_\nu\tilde{F}^{\mu\nu}) \equiv 2\partial_\mu D^\mu \tag{1.53}$$

is defined in terms of the total derivative of the dual current D^μ and does not affect the equations of motion. The infinitesimal form of the transformation (1.52)

$$\mathscr{L}_o \rightarrow \mathscr{L}_o - \partial_\mu D^\mu \delta\theta \tag{1.54}$$

gives the dual current conservation

$$\partial_\mu D^\mu = 0, \tag{1.55}$$

in agreement with the traditional theory.

This symmetry, also known as dual invariance, is a relevant feature of the classical electromagnetism and it is often used to argue that there is no need for the existence of monopoles. Dirac only proved that magnetic poles are not forbidden in quantum mechanics, but their existence is a significant argument of symmetry and also explains the charge quantization. If one looks at the non-free Maxwell's equations

$$\begin{aligned} \nabla\cdot\mathbf{E} = \rho_e, \quad \nabla\cdot\mathbf{B} = 0 \\ \nabla\times\mathbf{E} + \frac{\partial\mathbf{B}}{\partial t} = 0, \quad \nabla\times\mathbf{B} - \frac{\partial\mathbf{E}}{\partial t} = \mathbf{j}_e, \end{aligned} \tag{1.56}$$

where $\mathbf{j}_e$ is the electric current, the addition of a magnetic charge and the respectively transformation (1.49) give the new equations

$$\nabla\cdot(\mathbf{E} + i\mathbf{B}) = \rho_e + i\rho_g, \quad \nabla\times(\mathbf{E} + i\mathbf{B}) - i\frac{\partial}{\partial t}(\mathbf{E} + i\mathbf{B}) = \mathbf{j}_e + i\mathbf{j}_g, \tag{1.57}$$

where the charges are also invariant under the transformation

$$e + ig \rightarrow \mathrm{e}^{i\theta}(e + ig), \tag{1.58}$$

which could mean that the dual invariance does not imply that there are two different types of charge, but only one with an effective value

$$q = \sqrt{e^2 + g^2}. \tag{1.59}$$

This effective charge meets the concept of the dyon[5], a particle with both magnetic and electric charges whose theory has some similarities with the one proposed by Dirac[1][2]. However, the existence of a dyon does not imply that magnetic poles are banished, for they can be treated as dyons with no electric charge[39].

Chapter 2

The Magnetic Monopole in Field Theory

The quantization condition (1.11) is derived without any consideration about spin, even though Dirac[2] expected the magnetic monopole to be a spin 1/2 particle just like the electron. From now on the monopole will be treated as a spin 1/2 fermion for simplicity and in agreement with the previous symmetry arguments. A review of monopoles with spin 0 and 1 can be seen in [40] and [21].

2.1 Some Topics on QED

We will now review some of the fundamental topics of Quantum Electrodynamics (QED), the field theory used to describe the interaction of charged particles. We will start with the non-interacting Dirac field that describes a free particle with spin 1/2 and then include the electromagnetic interaction, culminating in the QED lagrangian, and from that the scattering matrices, Feynman rules and cross sections can be derived.

2.1.1 The Dirac Field

The lagrangian that describes the field of a free particle with spin 1/2 and mass m is given by

$$\mathscr{L} = -\bar{\psi}(\gamma^\mu \partial_\mu + m)\psi, \tag{2.1}$$

where γ^μ are the gamma matrices (A.12). The wavefunction $\psi(x)$ is the Dirac field, a spinor with four components and adjoint defined by

$$\bar{\psi}(x) \equiv \psi^\dagger(x)\gamma^0. \tag{2.2}$$

From the lagrangian (2.1) one can obtain the conjugate fields of $\psi(x)$ and $\bar{\psi}(x)$

$$\pi_\mu = \frac{\partial \mathscr{L}}{\partial \dot{\psi}_\mu} = -\psi^\dagger_\mu, \quad \bar{\pi}_\mu = \frac{\partial \mathscr{L}}{\partial \dot{\bar{\psi}}_\mu} = 0, \tag{2.3}$$

where the indice μ represents one of the four components of ψ and the dot a time derivative. Varying the action integral

$$S(\Omega) = \int_\Omega \mathscr{L}\, dx^4 \tag{2.4}$$

with respect to the field components ψ_μ and $\bar{\psi}_\mu$ we obtain the Dirac equation and its adjoint form, respectively

$$(\gamma^\mu \partial_\mu + m)\psi(x) = 0, \quad \text{and} \tag{2.5}$$

$$\bar{\psi}(x)(\gamma^\mu \partial_\mu - m) = 0. \tag{2.6}$$

In order to build a complete field theory for this particle of spin 1/2, the next step is to quantize the Dirac field ψ. Fixing $\mathbf{p}$ in (2.5), one can obtain independent solutions that can be written in the form (see (A.13) for notation)

$$(i\not{p} + m)u(\mathbf{p}, \sigma) = 0, \quad (-i\not{p} + m)v(\mathbf{p}, \sigma) = 0, \tag{2.7}$$

where $u(\mathbf{p}, \sigma)$ represents a particle with momentum p and spin σ ($\pm 1/2$) and $v(\mathbf{p}, \sigma)$ its antiparticle with momentum $-p$. With the appropriate choice of normalization, the total wave function can now be expanded in terms of these independent solutions

$$\begin{aligned}\psi_l(x) = \sum_{\sigma=\pm 1/2} (2\pi)^{-3/2} \int d^3p \, \big[& u_l(\mathbf{p}, \sigma) a(\mathbf{p}, \sigma) \mathrm{e}^{ip\cdot x} \\ & + v_l(\mathbf{p}, \sigma) a^\dagger(\mathbf{p}, \sigma) \mathrm{e}^{-ip\cdot x} \big] ,\end{aligned} \tag{2.8}$$

where the indice l indicates the spinor component and a and $a^\dagger$ are the annihilation and creation operators for fermions, respectively (see (A.8) and (A.10)). The conjugate field can also be written

$$\begin{aligned}\pi_l(x) = \sum_{\sigma=\pm 1/2} (2\pi)^{-3/2} \int d^3p \, [& a^\dagger(\mathbf{p}, \sigma) u_l^\dagger(\mathbf{p}, \sigma) \mathrm{e}^{-ip\cdot x} \\ & + a(\mathbf{p}, \sigma) v_l^\dagger(\mathbf{p}, \sigma) \mathrm{e}^{ip\cdot x}].\end{aligned} \tag{2.9}$$

The Electromagnetic Interaction

The usual procedure to describe the interaction of a relativistic electric charge with an electromagnetic field is to make the replacement

$$\partial_\mu \to D_\mu \equiv [\partial_\mu - iqA_\mu] \tag{2.10}$$

in (2.5), where q is the charge of the particle. We can now rewrite the lagrangian (2.1) as

$$\mathscr{L} = -\bar{\psi} \left[\not{D} + m \right] \psi. \tag{2.11}$$

Now we have a lagrangian that describes free particles with charge and their interaction with a magnetic field, but to build the full QED lagrangian one still needs to add a term representing free photons. Looking at the lagrangian of an electromagnetic field

$$\mathscr{L} = -\frac{1}{4} F^{\mu\nu} F_{\mu\nu} - j^\mu A_\mu, \tag{2.12}$$

we can see that the missing term is just

$$-\frac{1}{4} F^{\mu\nu} F_{\mu\nu}, \tag{2.13}$$

and the QED lagrangian can be written as

$$\mathscr{L} = \mathscr{L}_o + \mathscr{L}_I, \tag{2.14}$$

where

$$\mathscr{L}_o = -\bar{\psi}(\gamma^\mu \partial_\mu + m)\psi - \frac{1}{4}F^{\mu\nu}F_{\mu\nu} \tag{2.15}$$

represents the free fermions and photons and

$$\mathscr{L}_I = iq\bar{\psi}\not{A}\psi \tag{2.16}$$

is the interaction lagrangian.

2.1.2 S-matrix and the Feynman Rules

In a scattering process, the initial $|i\rangle$ and final $|f\rangle$ states of the multiple particles involved are defined in the limit when there is no more interaction, meaning

$$\begin{aligned} |i\rangle &= |\Phi(t \to -\infty)\rangle\,, \text{ and} \\ |f\rangle &= |\Phi(t \to \infty)\rangle\,. \end{aligned} \tag{2.17}$$

The scattering matrix, or S-matrix, relates these initial and final states and gives the probability for a certain process $i \to f$ to occur, and can be defined as

$$|f\rangle = S\,|i\rangle\,. \tag{2.18}$$

The transition probability between these two states will be given by

$$|S_{fi}|^2 \equiv |\,\langle f|S|i\rangle\,|^2, \tag{2.19}$$

and will respect the unitarity condition

$$\sum_f |S_{fi}|^2 = 1. \tag{2.20}$$

To construct the S-matrix, we first need to look at the time evolution of an arbitrary state vector $|\Phi(t)\rangle$:

$$i\frac{d}{dt}\,|\Phi(t)\rangle = H_I(t)\,|\Phi(t)\rangle\,, \tag{2.21}$$

where H_I is the interaction Hamiltonian

$$H_I(t) = \mathrm{e}^{iH_o(t-t_o)}H_I\mathrm{e}^{-iH_o(t-t_o)}, \tag{2.22}$$

with H_I and H_o the interaction and free hamiltonian in the Schrödinger picture, when there is no time dependence in the operators. Considering the initial state $|i\rangle$, (2.21) can be written in an integral form

$$|\Phi(t)\rangle = |i\rangle - i\int_{-\infty}^{t} H_I(t_1)\,|\Phi(t_1)\rangle\;dt_1. \tag{2.23}$$

Since we only know the initial condition, when $t \to \infty$, equation (2.23) can only be solved by iteration

$$|\Phi(t)\rangle = |i\rangle - i\int_{-\infty}^{t} H_I(t_1)\left[|i\rangle - i\int_{-\infty}^{t_1} H_I(t_2)\,|\Phi(t_2)\rangle\; dt_2\right] dt_1 \tag{2.24}$$

and so on, until we obtain the desired accuracy. Taking the limit $t \to \infty$, the S-matrix can be written

$$\begin{aligned} S =& \sum_{n=0}^{\infty}(-i)^n \int_{-\infty}^{\infty} dt_1 \int_{-\infty}^{t_1} dt_2 \cdots \int_{-\infty}^{t_n} H_I(t_1)H_I(t_2)\dots H_I(t_n) \\ =& \sum_{n=0}^{\infty} \frac{(-i)^n}{n!} \int_{-\infty}^{\infty} dt_1 \int_{-\infty}^{\infty} dt_2 \cdots \int_{-\infty}^{\infty} dt_n\, T\{H_I(t_1)H_I(t_2)\dots H_I(t_n)\}, \end{aligned} \tag{2.25}$$

where the term $n = 0$ corresponds to $\langle i|i\rangle = 1$ and T is the time-ordered operator, imposing that hamiltonians of later times stand to the left of hamiltonians with earlier times.

At this point we can note how the coupling constant of the theory plays a role in defining whether one is allowed to use perturbative methods or not. From the unitarity condition (2.20) the S-matrix has to be finite, and this can only be achieved in the iteration method if the contributions in the sum are small and get close to zero as $n \to \infty$. As can be seen from (2.16), the interaction hamiltonian of QED will be proportional to the coupling α (remember that $\alpha \sim e^2$), which is much smaller than one. From that, when n goes to infinity the infinite product of hamiltonians will imply that the exponent attached to α also goes to infinity, so that the contribution of these high order terms will eventually be considered as zero. If we had a coupling bigger than one, the contributions would grow with n and the S-matrix would not respect the unitarity condition.

Rewriting the S-matrix in terms of the hamiltonian density $\mathscr{H}$, the time integrals become integrals in all space time

$$S = \sum_{n=0}^{\infty} \frac{(-i)^n}{n!} \int\cdots\int d^4x_1 d^4x_2 \dots d^4x_n T\{\mathscr{H}_I(x_1)\mathscr{H}_I(x_2)\dots\mathscr{H}_I(x_n)\}, \tag{2.26}$$

and we can then write a general element of the matrix as

$$\begin{aligned} \langle f|S|i\rangle =& S_{\mathbf{p}_1'\sigma_1'n_1';\mathbf{p}_2'\sigma_2'n_2';\dots,\mathbf{p}_1\sigma_1n_1;\mathbf{p}_2\sigma_2n_2;\dots} \\ =& \sum_{n=0}^{\infty} \frac{(-i)^n}{n!} \int d^4x_1 \dots d^4x_n \big[\Phi_0, \dots a(\mathbf{p}_2'\sigma_2'n_2')a(\mathbf{p}_1'\sigma_1'n_1') \\ & \times T\left\{\mathscr{H}_I(x_1)\dots\mathscr{H}_I(x_n)\right\} a^\dagger(\mathbf{p}_1\sigma_1n_1)a^\dagger(\mathbf{p}_2\sigma_2n_2)\dots\Phi_0^\dagger\big], \end{aligned} \tag{2.27}$$

where $\mathbf{p}$, σ and n represents the particles momenta, spin and specie respectively. The prime denotes particles in the final state, Φ_0 is the free particle vacuum state and a and $a^\dagger$ are the annihilation and creation operators (see (A.8) and (A.10)), respectively.

From this definition, we can now start the derivation of the well-known Feynman Rules, a very useful tool to write amplitude matrices and, consequently, cross sections and many other kinematic features in scattering processes. As we are dealing

with a multiparticle state, each interaction hamiltonian can be written as[41]

$$\mathscr{H}_I(x) = \sum_i g_i \mathscr{H}_i(x), \tag{2.28}$$

where the sum is made over all species and $\mathscr{H}_i(x)$ can be written as a product of fields and field adjoints of the kind

$$\begin{aligned}\psi_l(x) = \sum_\sigma (2\pi)^{-3/2} \int d^3p \, \big[& u_l(\mathbf{p},\sigma,n) a(\mathbf{p},\sigma,n) \mathrm{e}^{ip\cdot x} \\ & + v_l(\mathbf{p},\sigma,n^c) a^\dagger(\mathbf{p},\sigma,n^c) \mathrm{e}^{-ip\cdot x} \big] ,\end{aligned} \tag{2.29}$$

where n^c denotes an antiparticle of species n and l labels the components of $\psi(x)$. For example, for a free particle of spin 1/2, u_l and v_l are the spinors (2.7) and $\psi(x)$ satisfies the Dirac equation (2.5). For a particle with spin 1 and no distinct antiparticle, like the photon, the fields can be written as

$$u^\mu(\mathbf{p},\sigma) = v^{\mu *}(\mathbf{p},\sigma) = \frac{e^\mu(\mathbf{p},\sigma)}{2|\mathbf{p}|}, \tag{2.30}$$

where e^μ are the polarization vectors that depend on the spin direction.

The process to obtain information from (2.27) starts with moving all the annihilation operators to the extreme right (but to the left of Φ_0) using the commutation relations (A.11). By definition, all the terms with an annihilation operator to the left of Φ_0 or a creation operator adjoint to the right of $\Phi_0^\dagger$

$$a(\mathbf{p},\sigma,n)\Phi_0 = 0, \quad \Phi_0^\dagger a^\dagger(\mathbf{p},\sigma,n) = 0 \tag{2.31}$$

will be zero, leaving only paired terms of both operators with delta functions for the momenta, spin and species numbers. Each term will have a definite product between the paired operators and the fields $\psi(x)$ and $\psi^\dagger(x)$, and all the possible combinations can be handled with the commutators

$$\begin{aligned}[a(\mathbf{p}',\sigma',n'), \psi_l^\dagger(x)]_\mp &= (2\pi)^{-3/2} \mathrm{e}^{-ip'\cdot x} u_l^*(\mathbf{p}',\sigma',n') \\ [a(\mathbf{p}',\sigma',n'^c), \psi_l(x)]_\mp &= (2\pi)^{-3/2} \mathrm{e}^{-ip'\cdot x} v_l(\mathbf{p}',\sigma',n') \\ [\psi_l(x), a^\dagger(\mathbf{p},\sigma,n)]_\mp &= (2\pi)^{-3/2} \mathrm{e}^{ip\cdot x} u_l(\mathbf{p},\sigma,n) \\ [\psi_l^\dagger(x), a^\dagger(\mathbf{p},\sigma,n^c)]_\mp &= (2\pi)^{-3/2} \mathrm{e}^{ip\cdot x} v_l^*(\mathbf{p},\sigma,n) \\ [a(\mathbf{p}',\sigma',n'), a^\dagger(\mathbf{p},\sigma,n)]_\mp &= \delta^{(3)}(\mathbf{p}' i\mathbf{p}) \delta_{\sigma'\sigma} \delta_{n'n},\end{aligned} \tag{2.32}$$

where the minus sign is for both particles being bosons, and the plus sign for fermions. The last possible combination is

$$\theta(x-y)[\psi_l^+(x), \psi_m^{+\dagger}(y)]_\mp \pm \theta(x-y)[\psi_m^{-\dagger}(y), \psi_l^-(x)]_\mp \equiv -i\Delta_{lm}(x,y), \tag{2.33}$$

where

$$\begin{aligned}\psi_l^+(x) &\equiv (2\pi)^{-3/2} \int d^3p \sum_\sigma u_l(\mathbf{p},\sigma,n) \mathrm{e}^{ip\cdot x} a(\mathbf{p},\sigma,n), \\ \psi_l^-(x) &\equiv (2\pi)^{-3/2} \int d^3p \sum_\sigma v_l(\mathbf{p},\sigma,n) \mathrm{e}^{-ip\cdot x} a^\dagger(\mathbf{p},\sigma,n^c)\end{aligned} \tag{2.34}$$

are the therms that destroy particles and create antiparticles in ψ, respectively, and the theta function $\theta(x-y)$ comes from the time-ordering operator and demands that $x^0 > y^0$.

The theory developed so far, except for the solution of the fields (2.5), (2.7) and (2.30), is quite general and can be applied for a several variety of fields. We will now focus on the derivation of the Feynman rules for Quantum Electrodynamics (QED), and then in the adjustments to include the magnetic monopole.

The Electron and Photon Propagators

To start the derivation of the Feynman rules for QED, it is necessary to write the propagators (2.33) for the electron and the photon. By substituting (2.34) in (2.33), one gets

$$\begin{aligned} -i\Delta_{lm}(x,y) =& \theta(x-y)(2\pi)^{-3}\int d^3p \sum_\sigma u_l(\mathbf{p},\sigma,n)u_m^*(\mathbf{p},\sigma,n)\mathrm{e}^{ip\cdot(x-y)} \\ &- \theta(y-x)(2\pi)^{-3}\int d^3p \sum_\sigma v_m^*(\mathbf{p},\sigma,n)v_l(\mathbf{p},\sigma,n)\mathrm{e}^{ip\cdot(y-x)}. \end{aligned} \tag{2.35}$$

For a particle of spin 1/2 and mass m like the electron or the monopole, the sums are given by [41]

$$\begin{aligned} \sum_\sigma u_l(\mathbf{p},\sigma)u_m^*(\mathbf{p},\sigma) &= \frac{[(-i\gamma_\mu p^\mu + m)i\gamma^0]_{lm}}{2\sqrt{p^0}} \\ \sum_\sigma v_l(\mathbf{p},\sigma)v_m^*(\mathbf{p},\sigma) &= \frac{[(i\gamma_\mu p^\mu - m)i\gamma^0]_{lm}}{2\sqrt{p^0}} \end{aligned} \tag{2.36}$$

where $p^0 = \sqrt{\mathbf{p}^2+m^2}$. The multiplication by $i\gamma^0$ is usually dropped off by using $\bar{\psi}$ (as in (A.14)) instead of $\psi^\dagger$. The electron propagator can then be written as (see (A.13) for notation)

$$-i\Delta_{lm}(x,y) = (2\pi)^{-3}\int d^3p \frac{[\not{p}+m]_{lm}}{2\sqrt{p^0}}[\theta(x-y)\mathrm{e}^{ip\cdot(x-y)} + \theta(y-x)\mathrm{e}^{ip\cdot(y-x)}] \tag{2.37}$$

To calculate the photon propagator, one can replace (2.30) in (2.8) to get

$$\begin{aligned} -i\Delta_{\mu\nu}(x-y) = \int \frac{d^3p}{(2\pi)^3 2\mathbf{p}} &\sum_{\sigma=\pm1} e_\mu(\mathbf{p}.\sigma)e_\nu^*(\mathbf{p},\sigma) \\ &\times \left[\mathrm{e}^{ip\cdot(x-y)}\theta(x-y) + \mathrm{e}^{ip\cdot(y-x)}\theta(y-x)\right] \end{aligned} \tag{2.38}$$

To get information from (2.38), it is necessary to study the electromagnetic potential and its constraints. Starting with the Lagrangian density of the free electromagnetic field (2.12), the Hamiltoninan can be written as

$$H = H_0 + V,$$

where

$$H_0 = \int \left[\frac{1}{2}\mathbf{\Pi}^2 + \frac{1}{2}(\nabla\times\mathbf{A})^2\right] d^3x \tag{2.39}$$

is a free field term, with $\mathbf{\Pi}$ the canonical conjugate to $\mathbf{A}$

$$\mathbf{\Pi} = \dot{\mathbf{A}} \tag{2.40}$$

and both submitted to the gauge constraints

$$\nabla \cdot \mathbf{\Pi} = \nabla \cdot \mathbf{A} = 0 \tag{2.41}$$

and commutation relations

$$\begin{aligned} [A^i(\mathbf{x}), \Pi_j(\mathbf{y})] &= i\delta^i_j \delta^{(3)}(\mathbf{x}-\mathbf{y}) + i\frac{\partial^2}{\partial x^j \partial x^i}\left(\frac{1}{4\pi|\mathbf{x}-\mathbf{y}|}\right), \\ [A^i(\mathbf{x}), A^j(\mathbf{y})] &= [\Pi_i(\mathbf{x}), \Pi_j(\mathbf{y})] = 0, \end{aligned} \tag{2.42}$$

where the indices i and j run from 1 to 3. At last, the potential term is given by

$$V = \int -\mathbf{j}\cdot\mathbf{A} + \frac{1}{2} j^0 A^0 \, d^3x. \tag{2.43}$$

To evaluate the evolution of the potentials with time, (2.43) can be written in the interaction picture

$$V(t) = \mathrm{e}^{iH_0 t} V[\mathbf{A}, \mathbf{\Pi}, \dots]_{t=0} \mathrm{e}^{-iH_0 t} = V[\mathbf{a}(t), \pi(t), \dots], \tag{2.44}$$

where the dots are for the matter fields and its conjugates. The interaction picture fields $\mathbf{a}(t)$ and $\pi(t)$ will respect the same constraints (2.40),(2.41) and commutation rules (2.42) for any time t. These restrictions and the evolution of the conjugate field

$$i\dot{\pi}_i(\mathbf{x}, t) = [\pi_i(\mathbf{x}, t), H_0],$$

give that $\mathbf{a}(\mathbf{x}, t)$ satisfies the usual wave equation

$$\Box\, \mathbf{a} = \left[\frac{\partial^2}{\partial t^2} - \nabla^2\right] \mathbf{a} = 0. \tag{2.45}$$

Taking $a^0 = 0$, the general solution for the four vector field is

$$\begin{aligned} a^\mu(x) =& (2\pi)^{-3/2} \int \frac{d^3p}{\sqrt{2|\mathbf{p}|}} \\ & \times \sum_\sigma [\mathrm{e}^{ip\cdot x} e^\mu(\mathbf{p}, \sigma) a(\mathbf{p}, \sigma) + \mathrm{e}^{-ip\cdot x} e^{\mu *}(\mathbf{p}, \sigma) a^\dagger(\mathbf{p}, \sigma)], \end{aligned} \tag{2.46}$$

with $a(\mathbf{p}, \sigma)$ and $a^\dagger(\mathbf{p}, \sigma)$ the annihilation and creation operators for bosons. The vectors $e^\mu(\mathbf{p}, \sigma = \pm 1)$ can be chosen to be the polarization vectors (2.30) and must satisfy the relations

$$\mathbf{p}\cdot\mathbf{e}(\mathbf{p}, \sigma) = 0, \quad e^0(\mathbf{p}, \sigma) = 0 \tag{2.47}$$

and normalization condition

$$\sum_{\sigma=\pm 1} e^i(\mathbf{p}, \sigma) e^{j*}(\mathbf{p}, \sigma) = \delta_{ij} - \frac{p_i p_j}{|\mathbf{p}|^2}. \tag{2.48}$$

The photon propagator can now be written as

$$-i\Delta_{\mu\nu}(x-y) = \int \frac{d^3p}{(2\pi)^3 2\mathbf{p}} \left(\eta_{\mu\nu} - \frac{p_\mu p_\nu}{|\mathbf{p}|^2}\right) \left[\mathrm{e}^{ip\cdot(x-y)}\theta(x-y) + \mathrm{e}^{ip\cdot(y-x)}\theta(y-x)\right]. \tag{2.49}$$

To drop off the theta functions and write the propagators in the usual form, their Fourier representations are used

$$\theta(t) = -\frac{1}{2\pi i}\int_{-\infty}^{\infty} \frac{\mathrm{e}^{-ist}}{s+i\epsilon}\, ds, \tag{2.50}$$

and the common factor in (2.37) and (2.49) can be arranged to give

$$\Delta_{lm}^{electron}(x-y) = (2\pi)^{-4}\int d^4q \frac{[-i\not{q}+m]_{lm}}{q^2-m^2-i\epsilon}\mathrm{e}^{iq\cdot(x-y)}, \tag{2.51}$$

$$\Delta_{\mu\nu}^{photon}(x-y) = (2\pi)^{-4}\int d^4q \frac{\eta_{\mu\nu}}{q^2-i\epsilon}\mathrm{e}^{iq\cdot(x-y)}, \tag{2.52}$$

where the new variable q is defined as $\mathbf{q} = \mathbf{p}$ and q^0 is chosen to give four-momentum conservation. The second term in the parenthesis of (2.49) is dropped to make an effective propagator[41].

Summary of the Rules and Cross Sections

The usual way to write the S-matrix and the Feynman rules is in momentum space, where all the exponential factors in (2.32),(2.51) and (2.52) will result in delta functions to ensure momentum conservation in each vertex after integration in the space-time coordinates. The S-matrix in momentum space can then be written as[42] (the indices f and $'$ stand for final states and i for initial states, for a clear notation)

$$\begin{aligned} S_{fi} =& \delta_{fi} + (2\pi)^4\delta^{(4)}\left(\sum p_f' - \sum p_i\right)\prod_i\left(\frac{1}{2VE_i}\right)^{1/2} \\ &\times\prod_f\left(\frac{1}{2VE_f'}\right)^{1/2}\mathscr{M}, \end{aligned} \tag{2.53}$$

where p and E are the four-momentum and energy of each initial or final particle, the index l runs for all initial and final leptons and V is the total integrated volume ($V\to\infty$). $\mathscr{M}$ is the Feynman amplitude, defined by

$$\mathscr{M} = \sum_{n=1}^{\infty}\mathscr{M}^{(n)}, \tag{2.54}$$

where each term $\mathscr{M}^{(n)}$ represents the nth order perturbation term in the S-matrix, and is written as the product of the corresponding Feynman rules, that after integration in momentum space can be summarized as follows:

- Vertices: label each vertex with an index μ, and for each vertex containing a pair of lepton and antilepton with charge q and a photon, include a factor $iq\gamma^\mu$

- External lines: label each external line with the particle momentum $\mathbf{p}$ and helicity or spin component index r

  1. For each final lepton going out of a vertex include a factor $\bar{u}_r(\mathbf{p})$
  2. For each final antilepton coming into a vertex include a factor $v_r(\mathbf{p})$
  3. For each initial lepton coming into a vertex include a factor $u_r(\mathbf{p})$
  4. For each initial antilepton going out of a vertex, include a factor $\bar{v}_r(\mathbf{p})$
  5. For each initial photon, coming into a vertex with label μ, include a factor $e_{r\mu}$
  6. For each final photon, going out of a vertex with label μ, include a factor $e^*_{r\mu}$

- Internal lines

  1. For each internal lepton with momentum k running from a vertex with label μ to another vertex with label ν, include a factor

$$i\frac{[\not{k}+m]_{\mu\nu}}{k^2-m^2} \tag{2.55}$$

  2. For each internal photon with momentum k running between two vertices with labels μ and ν, include a factor

$$-i\frac{\eta_{\mu\nu}}{k^2} \tag{2.56}$$

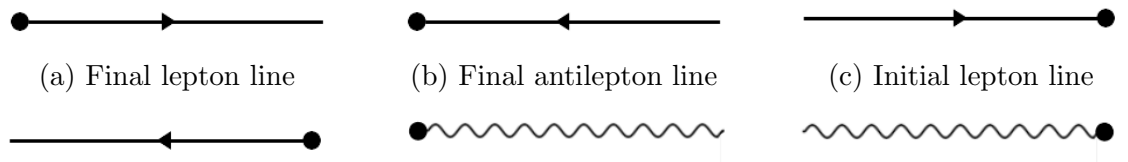

(a) Final lepton line (b) Final antilepton line (c) Initial lepton line

(d) Initial antilepton line (e) Final photon line (f) Initial photon line

Figure 2.1: External lines in a Feynman diagram

Each electron or photon line will be represented in the diagram according to Figure 2.1. The product of all these factors will be ordered so that, reading from right to left, they will follow the fermion lines. As we can see from the non-integrated rules, some of the factors $(2\pi)^{-4}$ will not cancel out after integration, and overall the Feynman amplitude will have a factor (for graphs without loops)[42]

$$(2\pi)^{4(n-f_i-b_i-1)},$$

where n is the number of vertices, f_i and b_i are the number of internal fermion and photon lines, respectively, and the -1 corresponds for the factor $(2\pi)^4$ in (2.53).

To obtain the differential cross section for a certain process, we need to multiply the transition probability (2.18) per time by the number of possible final states, in the limit where both the time interval and V go to infinity. For the particular case

of two incident particles (1 and 2) in the center of mass frame, the differential cross section takes the form[42]

$$d\sigma = (2\pi)^4 \delta^{(4)} \left(\sum p_f^{'} - \sum p_i \right) \frac{1}{4|\mathbf{p}_1|\sqrt{s}} \left(\prod_f \frac{d^3\mathbf{p}_f^{'}}{(2\pi)^3 2E_f^{'}} \right) |\mathscr{M}|^2, \tag{2.57}$$

where $\sqrt{s} = E_1 + E_2$ is the total center of mass energy of the system, in terms of the Mandelstan variable s (see (A.6)). Now, for the case of two particles in the initial and final states in the center of mass frame, the relations between momenta can be used to obtain a more usable form of the cross section

$$\frac{d\sigma}{d\Omega} = \frac{1}{64\pi^2 s} \frac{|\mathbf{p}_1^{'}|}{|\mathbf{p}_1|} |\mathscr{M}|^2, \tag{2.58}$$

where $\mathbf{p}_1^{'}$ and $\mathbf{p}_1$ are the momenta of the final and initial particles, respectively. In the next chapter we show the total cross sections for two of these processes, the photon fusion and Drell Yan, and as example, and the derivations of these cross sections are given in Appendix B.

2.2 Magnetic Monopole Couplings

2.2.1 Velocity Dependent Coupling

One easy way to handle the difficulty in using perturbative methods when dealing with magnetic monopoles is to suppose a velocity dependent coupling

$$\alpha_m = \frac{\beta^2 g^2}{4\pi}, \tag{2.59}$$

where β is the monopole velocity. This way, the moving magnetic monopole is treated as an electric charge, in analogy with the fact that a moving electric charge behaves as a source of magnetic field. With this coupling, the field Lagrangian for monopole interaction with photons is written as

$$\mathscr{L}_\beta = -\frac{1}{4} F_{\mu\nu} F^{\mu\nu} + \bar{\psi}(i\not{\mathscr{D}} - m)\psi, \tag{2.60}$$

where

$$\not{\mathscr{D}} = \gamma^\mu [\partial_\mu - ig\beta A_\mu]. \tag{2.61}$$

The Lagrangian (2.60) is just the QED lagrangian for a particle with mass m and electric charge $g\beta$, with γ^μ the gamma matrices (A.12) and $\psi(x)$ the solution of Dirac equation (2.5). However, due to the large value of g, the perturbation methods of the previous section can only be used in the limit

$$\beta \ll 1. \tag{2.62}$$

Even in this limit the simulations obtained using the Feynman rules are only indicative, but useful to obtain estimated predictions until there is no formal theory describing magnetic monopole interactions.

2.2.2 Magnetic Moment for the Monopole

The magnetic moment of an electron with spin vector **S** is given by

$$\mu_e = -g_e \frac{e}{2m}\mathbf{S}, \tag{2.63}$$

where

$$g_e = 2\left(1 + \frac{\alpha}{2\pi}\right) \approx 2.002$$

is the electron gyromagnetic ratio[42]. The electron magnetic moment does not appear directly on the tree-level (first order) QED Lagrangian, but it is generated through the scattering of the electron by a magnetic field and contributes only in higher order graphs, as in Fig. 2.2 . Because of its low value, the electron magnetic moment is only relevant when considering high order diagrams that contain radiative corrections.

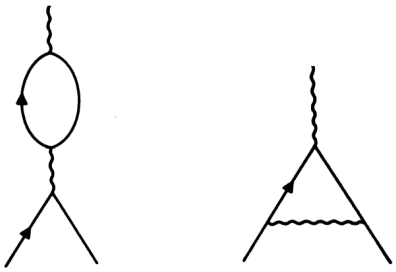

Figure 2.2: Finite contributions of radiative corrections in an electron scattering by an external magnetic field[42]

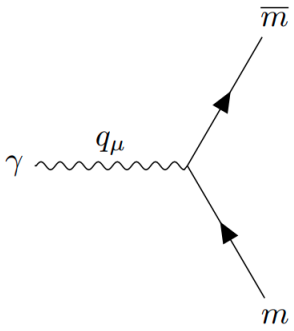

Figure 2.3: Monopole-photon interaction vertex.

An alternative to the simple velocity-dependent coupling is to consider a magnetic moment term added in the lagrangian (2.60). As the monopole itself generates a magnetic field, it would not be necessary an electromagnetic scattering to generate magnetic moment. Also, due to the large value of g, the monopole can be expected to have a great magnetic moment, and it would be relevant already in a tree-level diagram. The new Lagrangian can be written as[21]

$$\mathscr{L}_{\kappa\beta} = \mathscr{L}_\beta - \frac{i}{4} g\beta\kappa F_{\mu\nu}\bar{\psi}[\gamma^\mu, \gamma^\nu]\psi, \tag{2.64}$$

with κ composing the magnetic moment of the monopole

$$\mu_m = \frac{g\beta}{2m} 2(1 + 2\tilde{\kappa})\hat{S}, \tag{2.65}$$

where $\tilde{\kappa} = \kappa m$ and $\hat{S} = 1/2$. Now the photon-monopole coupling will be proportional to

$$\propto -ig\beta(\gamma^\mu) + \frac{\kappa}{2} q_\mu [\gamma^\mu, \gamma^\nu], \tag{2.66}$$

where q_μ is the photon momentum (see Fig. 2.3). Considering the magnetic moment couplings and that the monopole magnetic momentum is given by (2.65), a perturbatively small coupling will require that[21]

$$(g\beta)(\kappa m\beta) = g\tilde{\kappa}\beta^2 < 1, \tag{2.67}$$

which can be achieved with the limits

$$\tilde{\kappa} \gg 1 \quad \text{and} \quad \beta \ll 1. \tag{2.68}$$

Chapter 3

Monopole Production

3.1 Photon Fusion

3.1.1 Elementary Photon Fusion Processes

The $\gamma\gamma$ (two photon) fusion processes has been useful for studying the production of charged leptons, the Higgs boson[23][24] and particles beyond the Standard Model, like supersymmetry charged scalar particles[25]. A general process of photon fusion is depicted in Figure 3.1, where two initial charged particles (electrons, quarks, protons...) emit one photon each, and the two photons interact to produce new particles. For electrons or quarks this is a typical scattering process, while protons or other hadrons can disintegrate to form a distinct final state. The blob in Figure 3.1 represents the interactions between the photons to form the final particles. For a spin 1/2 lepton pair production (lepton + antilepton), the interaction can occur in two ways, via t-channel or u-channel, as shown in Figure 3.2.

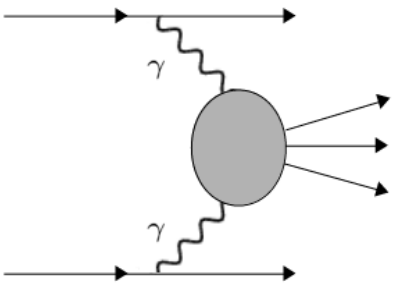

Figure 3.1: General process of photon fusion.

The cross section for lepton pair production is obtained using the Feynman rules and the cross section formalism described in Chapter 2, and is given by

$$\hat{\sigma}_{\gamma\gamma\to l^+l^-}(\hat{s}) = \frac{4\pi\alpha_l^2\beta}{\hat{s}}\left[\frac{3-\beta^4}{2\beta}\ln\frac{1+\beta}{1-\beta} - (2-\beta^2)\right], \tag{3.1}$$

where α_l is the coupling of the lepton with the photon, which for electrons or other electrically charged particles is simply the electromagnetic coupling α, and

$$\beta = \sqrt{1-4m^2/\hat{s}} \tag{3.2}$$

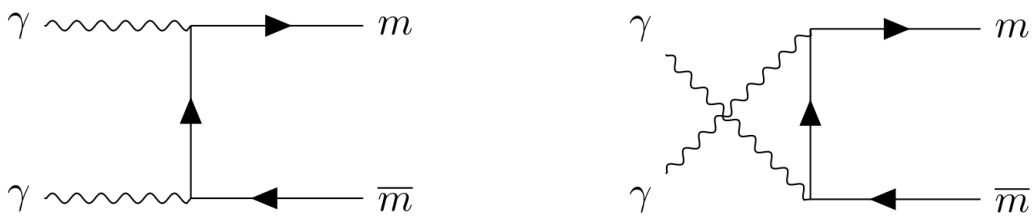

(a) t-channel. (b) u-channel.

Figure 3.2: Lepton pair production by photon fusion

is the lepton velocity ($c = 1$), with m its mass and $\sqrt{\hat{s}}$ the center of mass energy of the interaction. The hat over the variables s and σ indicates that they correspond to a subprocess to be considered in a more general collision, e.g. between protons and nuclei, so that the total cross section will depend on them. A detailed derivation of (3.1) is given in Appendix B.

3.1.2 Monopole Pair Production

Considering that monopoles couple to photons with the velocity dependent coupling $g\beta$, the cross sections for monopole production can be derived by the replacement

$$\alpha = \frac{e^2}{4\pi} \to \alpha_m = \frac{g^2\beta^2}{4\pi}. \tag{3.3}$$

in equation (3.1). Using the Dirac quantization condition (1.11), the magnetic coupling can also be written in the form

$$\alpha_m = \frac{n^2\beta^2}{4\alpha}. \tag{3.4}$$

Making the replacement, the cross section for monopole pair production by photon fusion becomes

$$\begin{aligned} \hat{\sigma}_{\gamma\gamma\to m\bar{m}}(\hat{s}) &= \frac{4\pi\alpha_m^2\beta}{\hat{s}}\left[\frac{3-\beta^4}{2\beta}\ln\frac{1+\beta}{1-\beta} - (2-\beta^2)\right] \\ &= \frac{\pi n^4\beta^5}{4\alpha^2\hat{s}}\left[\frac{3-\beta^4}{2\beta}\ln\frac{1+\beta}{1-\beta} - (2-\beta^2)\right]. \end{aligned} \tag{3.5}$$

The integer n will give the magnetic charge of the monopole in terms of the unitary charge in equation (1.12). In this work we choose to work only with the unitary charge, as it gives the lower cross sections and thus can generate more reliable limits on the monopole production. In the lower limits given by MoEDAL[18], considering both Drell Yan and photon fusion for the coupling $g\beta$, the limits increase with n due to the larger cross sections. In ATLAS[28], only the Drell Yan production is considered for the coupling g, and for this case the limits decrease with n, as we shall see in Sec. 3.2 that larger values of n give higher cross sections, although they are still small compared to photon fusion.

If the monopole-photon coupling depends on the monopole velocity and magnetic moment, a new cross section has to be formulated. The QED vertex factor $iq\gamma^\mu$ will now be (2.66) for both u and t channels, and the Feynman amplitudes will have

extra terms to incorporate the κ dependence. In [21] the cross section is derived using MadGraph algorithms[43] and is given by ($n = 1$ in (1.11))

$$\begin{aligned}\hat{\sigma}_{\gamma\gamma\to m\bar{m}}(\hat{s},\kappa) =& \frac{\pi\alpha_m^2(\beta)}{3\hat{s}}\Bigg\{\ln\left(\frac{1-\beta}{1+\beta}\right)\Big[\beta^2\kappa^2\hat{s}(3\beta^2\kappa^2\hat{s}-6\kappa^2\hat{s}+6)+6\beta^4 \\ & -(36\beta^2-72\beta)\kappa\sqrt{(1-\beta^2)\hat{s}}-9\kappa^4\hat{s}^2-60\kappa^2\hat{s}-18\Big] \\ & -\beta\kappa^2\hat{s}(7\beta^2\kappa^2\hat{s}^2+15\kappa^2\hat{s}+132)+12\beta^3-24\beta-36\kappa\sqrt{(1-\beta^2)\hat{s}}\Bigg\}\end{aligned} \tag{3.6}$$

For the case $\kappa = 0$, it recovers (3.5). The main objective of introducing the magnetic moment is to be able to use perturbative methods in more limiting cases rather than only $\beta \ll 1$. For the theory without κ, this limit will take the cross sections and also the probability of observation to zero. In the limit (2.68), the cross section (3.6) becomes

$$\lim_{\substack{\kappa\to\infty\\ \beta\to 0}} \hat{\sigma}_{\gamma\gamma\to m\bar{m}}(\hat{s},\kappa) = -5\pi\alpha_m^2(\beta)\kappa^4\hat{s} \sim \frac{(\tilde{\kappa}g\beta)^4\beta}{16\pi m^4}, \tag{3.7}$$

which is finite and goes to zero slower than β^2.

In Figure 3.3 we show the different cross sections for each model. As mentioned before, the velocity dependent coupling gives the lowest cross section, and for smaller values of β the difference between the models $\alpha_m \propto g^2\beta^2$ and $\alpha_m \propto g^2$ tends to get more significant. For the κ model, which also has a dependence in β, the order of magnitude of the cross sections heavily depend on the value of the parameter $\tilde{\kappa}$, and for $\tilde{\kappa} > 11$ it already gives higher cross sections than the $\alpha_m \propto g^2$ model.

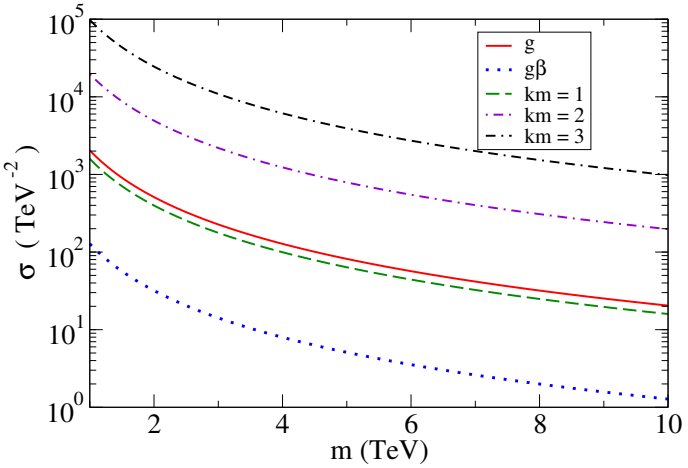

Figure 3.3: Comparison between the cross sections for the magnetic couplings g, $g\beta$ and the magnetic moment dependent with different values for the parameter $\tilde{\kappa} = \kappa m$, as function of the monopole mass m with $\beta = 0.5$ for an intermediary analysis.

3.1.3 Monopolium Production

The monopolium is a hypothetical bound state between a monopole and a anti-monopole, first proposed in [12] as a possible relic of magnetic monopoles pro-

duced in the early universe. Because of the great magnetic coupling, a monopole-antimonopole pair will probably annihilate into a pair of photons [16][44] or form a monopolium, which can have a small mass and more stability. For a spin 1/2 monopole, the monopolium can assume two spin values, 0 and 1, but in this work we choose to work with the spin 0 monopolium in order to consider the simplest and lowest energy case.

The monopolium is characterized by a binding energy $E_{binding}$ and its mass M, both related to the monopole mass m by the expression

$$M = 2m + E_{binding}. \tag{3.8}$$

For the spin 0 monopolium, the elementary subprocess for photon fusion is depicted in Figure 3.4, where $V(r)$ is the interaction potential that bounds the monopole pair.

Considering the monopolium to be an unstable intermediate state with a small decay rate, its production cross section will exhibit a peak at the monopolium mass, known as resonance. The general resonance cross section, derived in Appendix B, is given by

$$\hat{\sigma}(E) = \frac{4\pi}{E^2} \frac{M^2\Gamma(E)\Gamma}{(E^2 - M^2)^2 + M^2\Gamma^2}, \tag{3.9}$$

with $E = \sqrt{\hat{s}}$, Γ the total decay width of the monopolium and $\Gamma(E)$ the decay width into the initial state.

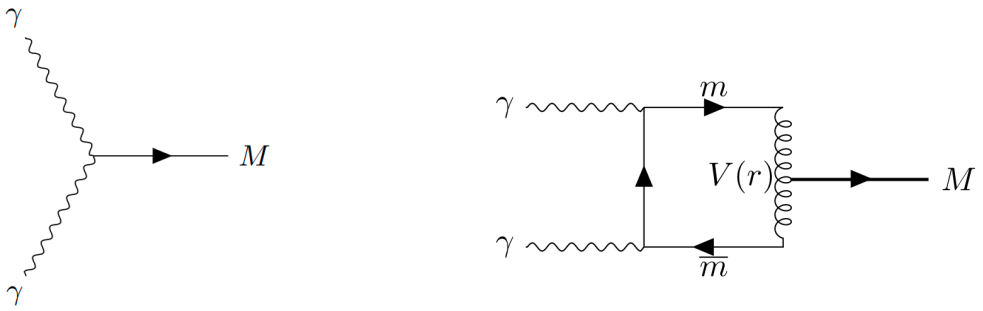

(a) Feynman graph

(b) Diagrammatic representation of the bound state

Figure 3.4: Elementary subprocess of monopolium production by photon fusion.

For the monopolium production by photon fusion, as depicted in Figure 3.4, we can write the decay width (B.33) as [16]

$$\Gamma_{\gamma\gamma\to M}(E) = \frac{32\pi\alpha_g^2(\beta)}{M^2} |\psi_M(0)|^2, \tag{3.10}$$

where the dependence in β comes from the interaction between the photons and monopoles, as in Figure 3.4b.

To write the monopolium wave function ψ_M, the interaction potential in the pair has to be known. Because of the great coupling between the monopole and its antiparticle, it is possible to argue that both have some spatial extension[45], so that the interaction is non-singular when their separation (r) goes to zero. This can be described with the potential[46]

$$V(r) = -g^2 \left(\frac{1 - \mathrm{e}^{-\mu r}}{r} \right), \tag{3.11}$$

where $\mu = 2m/g^2$ is the cut-off parameter that describes the interaction when $r \to 0$,

$$\lim_{r\to 0} V(r) \approx -g^2\mu = -2m, \tag{3.12}$$

which is the minimum energy for the system. When the separation is big enough, the potential has the usual behavior

$$\lim_{r\to\infty} V(r) = -\frac{g^2}{r}. \tag{3.13}$$

The binding energy is obtained by solving the Schrödinger equation with (3.11), and it is given by (with $n = 1$ in (1.11))

$$E_{bind} = -\left(\frac{1}{8\alpha}\right)^2 \frac{m}{N^2}, \tag{3.14}$$

where N is the principal quantum number, so that the monopolium mass is

$$M = 2m - \left(\frac{1}{8\alpha}\right)^2 \frac{m}{N^2}. \tag{3.15}$$

Because M has to be always positive, N will have a minimum value depending on the monopole mass m. Considering the monopolium to be in its ground state, with null spin and angular momentum, the wave function will be

$$|\psi_{N,0,0}(0)| = \frac{1}{4}\left(\frac{m}{2\alpha N}\right)^{3/2}, \tag{3.16}$$

and we can replace the relation between M and N (3.15) to get

$$|\psi_M(0)|^2 = 4\left(2 - \frac{M}{m}\right)^{3/2} m^3. \tag{3.17}$$

The production rate can then be written as

$$\Gamma(E) = \frac{2\beta^4}{M^2\alpha^2}\left(2 - \frac{M}{m}\right)^{3/2} m^3. \tag{3.18}$$

Defining $R = 2m/M$, $\bar{\Gamma} = \Gamma/M$ and $\epsilon = \sqrt{\hat{s}}/M$, the cross section can finally be written [47]

$$\hat{\sigma}_{\gamma\gamma\to M}(\hat{s}) = \frac{2\sqrt{2}[R(R-1)]^{3/2}}{\alpha^2\epsilon^6 M^2}\frac{\bar{\Gamma}(\epsilon^2-1)^2}{(\epsilon^2-1)^2+\bar{\Gamma}^2}. \tag{3.19}$$

An illustration of the behavior of the resonance cross section (3.19) is displayed in Figure 3.5. The peak occurs right after the monopolium mass $M = 1$ TeV, and the function rapidly decays with the increase of ϵ.

3.2 Drell Yan

3.2.1 Elementary Drell Yan Processes

The Drell Yan process[26] is characterized by the annihilation of a quark and its antiquark to form final particles. Like photon fusion, Drell Yan has been studied

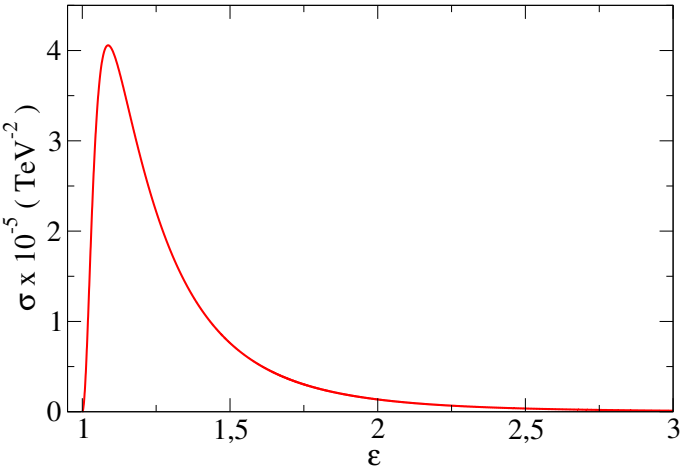

Figure 3.5: Cross section for the monopolium production as function of ϵ, with $M = 1$ TeV and $m = 3$ TeV.

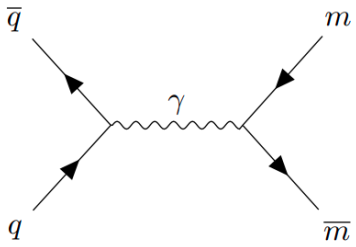

Figure 3.6: Lepton pair production by Drell Yan.

for the production of many charged fermions in supersymmetry models and also the Higgs boson[27]. Figure 3.6 shows the production of a pair $m\bar{m}$ of spin 1/2 leptons, which can occur in any collision involving hadrons. In the specific case of a proton-antiproton collision, the Drell Yan cross sections are greatly enhanced due to the presence of valence antiquarks.

In leading order (tree-level) the subprocess $q\bar{q} \to l\bar{l}$ can be studied considering only electromagnetic interactions, and the cross section can be derived from the Feynman graph in Fig. 3.6

$$\hat{\sigma}_{q\bar{q}\to l\bar{l}}(\hat{s}) = \frac{\pi\eta_q^2\alpha\alpha_l}{9\hat{s}}\frac{\beta_l}{\beta_q}\left[9 - 3(\beta_l^2 + \beta_q^2) + \beta_l^2\beta_q^2\right], \tag{3.20}$$

with η_q the fraction of the electric charge carried by the quark q, β_l and β_q the boosts of the leptons and quarks, respectively. The coupling α_l corresponds to the coupling of the lepton with the photon, and is written in this format so that it will be easier to generalize for monopoles. The derivation of this cross section is shown in Appendix B.

3.2.2 Monopole Pair Production

The cross section for monopole production is obtained in the same way as for lepton production, with the monopole charge $g\beta$ replacing the electric charge. However, the monopole mass is expected to be bigger than all quark masses so they can

be neglected, meaning that $\beta_q \to 1$ in (3.20)[21]. Using the Dirac's quantization condition we can write the monopole coupling α_m in terms of α as in (3.4), and the cross section will become, for each quark flavor,

$$\hat{\sigma}_{q\bar{q}\to m\bar{m}}(\hat{s}) = \frac{2\pi\eta_q^2\beta^3}{9\hat{s}}\left(3-\beta^2\right), \tag{3.21}$$

where $\beta \equiv \beta_l$ is the monopole boost.

To include the κ dependence, new Feynman amplitudes have to be derived, and the cross section can again be derived by using computational methods as in[21]. The cross section for each quark flavor will be given by

$$\hat{\sigma}_{q\bar{q}\to m\bar{m}}(\hat{s},\kappa) = \frac{2\pi\eta_q^2\beta^3}{9\hat{s}}\left[3-\beta^2-(2\beta^2-3)\kappa^2\hat{s}+6\kappa\sqrt{\hat{s}-\beta^2\hat{s}}\right], \tag{3.22}$$

where again it is used that $\beta_q \to 1$.

The comparison between the models in shown in Figure 3.7. Again the $g\beta$ model gives the lowest cross section, but now it is closer to the g curve than in the photon fusion case. The κ model gives higher cross sections than the non-effective model for the three values of $\tilde{\kappa}$ considered, and the order of magnitude of the cross section is nearly the same for all of them.

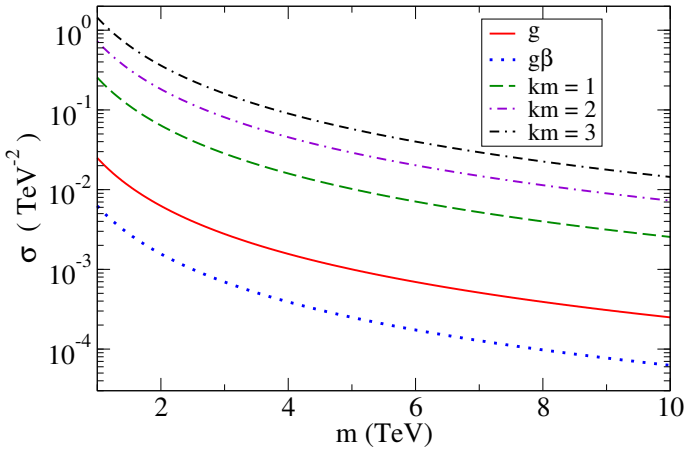

Figure 3.7: Comparison between the cross sections for the magnetic couplings g, $g\beta$ and the magnetic moment dependent with different values for the parameter $\tilde{\kappa} = \kappa m$, as function of the monopole mass m with $\beta = 0.5$ for an intermediary analysis.

Instead of enhanced, the DY cross section for monopole pair production is suppressed compared to the $\gamma\gamma$ process. This can be seen in a simple way by comparing the ratio of electromagnetic couplings in lepton production cross sections for $\gamma\gamma$ relative do DY

$$r_l = \frac{\gamma\gamma_{\text{couplings}}}{\text{DY}_{\text{couplings}}} = \frac{\bar{\eta}^4 e^4\alpha^2}{\bar{\eta}^2\alpha^2} = (4\pi\bar{\eta})^2\alpha^2, \tag{3.23}$$

where $\bar{\eta}$ is the average fraction of the electric charge carried by quarks, and the term $\bar{\eta}^4 e^4$ in the $\gamma\gamma$ cross sections is due to the inelastic contribution (see eqs. (4.7) and (4.20)). For the monopole production, the ratio will be

$$r_m = \frac{\bar{\eta}^4 e^4\alpha_m^2}{\bar{\eta}^2\alpha\alpha_m} = (4\pi\bar{\eta})^2\alpha\alpha_m \tag{3.24}$$

The ratio of the ratios gives

$$\frac{r_m}{r_l} = \frac{\alpha_m}{\alpha} = \frac{\beta^2}{\alpha^2}, \tag{3.25}$$

which can be very large if β is not too small. For lepton production, it was found[27] that, for a lepton mass $m_l = 100$ GeV and LHC energies, the $\gamma\gamma$ cross section is nearly 10^2 below the Drell-Yan cross section. With $\beta = 1$, this implies that the $\gamma\gamma$ will dominate the DY cross section by a factor of ~ 50 for monopole production.

Chapter 4

pp Collisions

4.1 Photon Flux

4.1.1 The Weizsäcker-Williams Method

The Weizsäcker-Williams method[48] consists in treating a charged particle in movement as a flux of virtual photons, that then will interact with a target in a photoproduction process. The method can be understood by figuring out the following scenario: in two inertial frames, S and S', with relative velocity in the x_1 direction, the Lorentz transformations for the electromagnetic fields will be[49]

$$\begin{aligned} E_1 = E_1^{'} \quad & B_1 = B_1^{'} \\ E_2 = \gamma(E_2^{'} + \beta B_3^{'}) \quad & B_2 = \gamma(B_2^{'} - \beta E_3^{'}) \\ E_3 = \gamma(E_3^{'} - \beta B_2^{'}) \quad & B_3 = \gamma(B_3^{'} + \beta E_2^{'}), \end{aligned} \tag{4.1}$$

where $\gamma = \frac{1}{\sqrt{1-\beta^2}}$ and β equals the relative velocity between the frames. If a particle with charge q is moving with constant velocity v in the x_1 direction in S, an observer at the point P in the coordinates $\mathbf{r}' = (-vt', h, 0)$ (see Fig. 4.1) in S' will sense the electric and magnetic fields

$$\begin{aligned} E_1^{'} = -\frac{qvt'}{r'^3}, \quad & B_1^{'} = 0 \\ E_2^{'} = \frac{qh}{r'^3}, \quad & B_2^{'} = 0 \\ E_3^{'} = 0, \quad \text{and} \quad & B_3^{'} = 0. \end{aligned} \tag{4.2}$$

For the same observer, the relation between the time in the two frames will be

$$t' = \gamma\left(t - \beta x_1\right) = \gamma t, \tag{4.3}$$

and the electric field in terms of S coordinates can be written

$$\begin{aligned} E_1^{'} &= -\frac{qh}{(h^2 + \gamma^2 v^2 t^2)^{3/2}}, \\ E_2^{'} &= -\frac{qh}{(h^2 + \gamma^2 v^2 t^2)^{3/2}}, \\ E_3^{'} &= 0. \end{aligned} \tag{4.4}$$

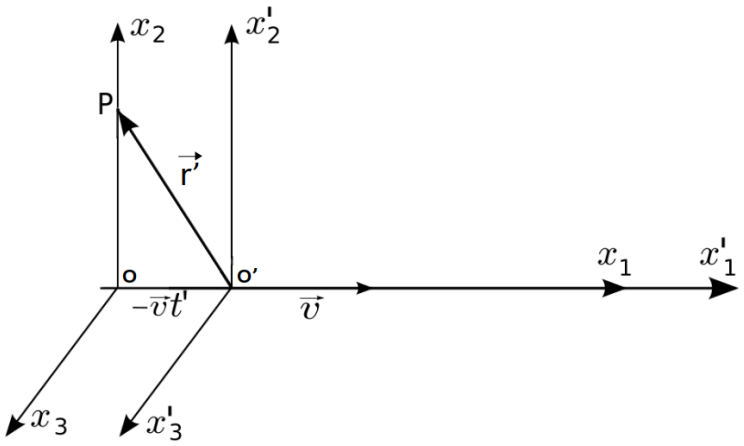

Figure 4.1: Charged particle at the origin of the frame S' moving with velocity **v** relatively to the frame S.

Replacing (4.4) into (4.2) and (4.1), one has the nonzero electromagnetic field components for an observer at the point P in S frame:

$$\begin{aligned} E_1 &= -\frac{q\gamma v t}{(h^2+\gamma^2 v^2 t^2)^{3/2}}, \\ E_2 &= \frac{\gamma q h}{(h^2+\gamma^2 v^2 t^2)^{3/2}}, \\ B_3 &= \beta E_2. \end{aligned} \tag{4.5}$$

In the ultrarelativistic limit ($\beta \sim 1$), the intensities of the magnetic field in the x_3 axis will be the same as the electric field in the x_2 axis. This symmetry provides a justification for the method, as the observer in S system will not be able to distinguish if the electromagnetic field is due to a charged particle in movement or to a simple radiation pulse. With this treatment, the cross section for photon production can be factorized to a density of photons f_γ times the photon-target cross section

$$\sigma = \int f_\gamma(\omega)\hat{\sigma}_\gamma(\omega)\, d\omega, \tag{4.6}$$

where ω is the photon energy. The aim is now resumed to obtain the necessary photon fluxes for the interactions in study.

4.1.2 The equivalent photon flux

The photoproduction in proton collisions can occur in three different ways: elastic, semielastic and inelastic. For each one, different photon fluxes will be used, as shown below

Inelastic photon flux

In the inelastic or semielastic collisions, both or one of the protons, respectively, disintegrate to form an unknown final state. An approximation to calculate the inelastic part of the cross sections is to use the parton model, that considers the proton as a sea of quarks, antiquarks and gluons that will freely interact with the

target. This configuration is only possible when one has ultrarelativistic protons with high momentum transfer, like in the LHC, and the strong coupling α_s is close to zero[50].

When dealing with photoproduction in inelastic interactions, the flux of photons will come from the relativistic charged quarks. In the limit where strong interactions can be neglected, the photon flux of a quark will be approximately equal to the flux of a relativistic electron[27]

$$f_{\gamma/q}(x) = \frac{\eta_q^2 e^2 \alpha}{2\pi} \frac{[1+(1-x)^2]}{x} \ln\left(\frac{Q_1^2}{Q_2^2}\right), \tag{4.7}$$

where x is the fraction of the quark (electron) energy carried by the photon. $Q^2 = -q^2$ is proportional to the photon momentum q, and Q_1 and Q_2 are its maximum and minimum values. Since we choose the scale $Q^2 = \hat{s}/4$ for the structure function of the proton (see next section) the maximum value will be $Q_1^2 = \hat{s}/4 - m^2$, where m is the mass of the produced particles (after interaction), and the minimum value is set to 1 GeV^2, in order for the free-parton configuration be applied.

The expression (4.7) used in [27] can be seen as an approximation of the expression for the flux of photons of a scattered electron given in [51]

$$x f_{\gamma/e}(x) = \frac{\alpha}{\pi}\left(1 - x + \frac{x^2}{2}\right)\ln\frac{Q_1^2}{Q_2^2} - \left(1-\frac{x}{2}\right)^2\left(\frac{x^2\hat{s}+Q_1^2}{x^2\hat{s}+Q_2^2}\right) - \frac{m_e^2 x^2}{Q_2^2}\left(1-\frac{Q_2^2}{Q_1^2}\right). \tag{4.8}$$

The approximation is valid in the high energy limit, where the first term $\propto \ln(Q_1^2/Q_2^2)$ will dominate over the last two terms.

Elastic photon flux

In elastic and semielastic collisions, both or one of the protons remains intact after the interaction, respectively. Since the proton does not disintegrate into a sea of quarks and gluons, the emitted photons will depend on the proton structure. This elastic photon flux can be obtained by considering the example of an ep scattering $ep \to Xp$, as done in [52]. For this process, the amplitude matrix will have the format

$$|\bar{\mathscr{M}}|^2 = \frac{1}{q^4} H^{\mu\nu}(p,q) T_{\mu\nu}(p_e, q; p_X), \tag{4.9}$$

with $T_{\mu\nu}$ containing all the information about the subprocess $e\gamma \to X$, with p_e and q the electron and photon momenta, respectively, and $H^{\mu\nu}$ the hadronic tensor for a proton with initial momentum p

$$H^{\mu\nu}(p,q) = 2e^2\left[\frac{G_E^2 - \frac{q^2}{4m^2}G_M^2}{1-\frac{q^2}{4m^2}}(2p-q)^\mu(2p-q)^\nu + G_M^2(q^2\eta^{\mu\nu} - q^\mu q^\nu)\right]. \tag{4.10}$$

The functions $G_E(q^2)$ and $G_M(q^2)$ are usually called electric and magnetic form factors, respectively, and are written in terms of the proton structure functions $F_1(q^2)$ and $F_2(q^2)$ that depend on the quark distribution inside the proton[54]. They can be written as

$$G_E(q^2) = F_1(q^2) + \frac{q^2}{4m^2}F_2(q^2) \;\text{ and }\; G_M(q^2) = F_1(q^2) + F_2(q^2), \tag{4.11}$$

and are well parameterized by the dipole form factor that gives

$$G_E(q^2) = \frac{1}{\left(1 - \frac{q^2}{0.71\,\mathrm{GeV}^2}\right)^2} \quad \text{and} \quad G_M(q^2) = 2.79 G_E(q^2). \tag{4.12}$$

To obtain the elastic photon flux, it is necessary to write the cross section in the form of the Weizsäcker-Williams approximation(4.6) in the high energy limit ($\hat{s} \gg m_p^2$). All the information about the final state X will be contained in the cross section, and the flux will be given by[52]

$$f^{el}_{\gamma/p}(z) = \frac{\alpha z}{2\pi} \int_{t_1}^{t_2} \left\{ 2\left[\frac{1}{z}\left(\frac{1}{z} - 1\right) - \frac{m_p^2}{Q^2}\right] \frac{G_E^2 + \frac{Q^2}{4m_p^2} G_M^2}{1 + \frac{Q^2}{4m_p^2}} + G_M^2 \right\} \frac{dQ^2}{Q^2}, \tag{4.13}$$

where $z = \hat{s}/s$ is the fraction of energy carried by the photon and $Q^2 = -q^2$ is the usual momentum transfer scale. The integration limits are obtained to constrain the interaction in the elastic regime and are given by

$$t_1 = \frac{(z m_p)^2}{1 - z} \quad \text{and} \quad t_2 = s(1 - z). \tag{4.14}$$

An analytic approximation for (4.13) is presented in [53]

$$f^{el}_{\gamma/p}(z) = \frac{\alpha}{2mz}[1 + (1 - z)^2] \left[\ln A - \frac{11}{6} + \frac{3}{A} - \frac{3}{2A^2} + \frac{1}{3A^3}\right], \tag{4.15}$$

where

$$A = 1 + \frac{0,71(GeV)^2}{Q_o^2}, \tag{4.16}$$

and

$$\begin{aligned} Q_o^2 = &-2m_p^2 + \frac{1}{2s} \\ &\times \left[(s + m_p^2)(s - zs + m_p^2) - (s - m_p^2)\sqrt{(s - zs - m_p^2)^2 - 4m_p^2 zs}\right]. \end{aligned} \tag{4.17}$$

A comparison between the two expressions is shown in Figure 4.2. The peak of R indicates an utmost difference of one order of magnitude, which is acceptable in the simulations performed in this work. Hence, we choose to work with the analytical form for computational purposes.

4.2 pp Collisions

The collision of two ultrarelativistic protons can generate several processes involving photons, quarks and gluons and has a cleaner sign than a collision between a proton and a nucleus or two nucleus. Proton beams at LHC are also more energetic than nuclei beams and can produce heavier particles up to a few TeV, which is the expected mass range of the monopole. A study of monopole production in nucleus collisions can be seen in [55], and as noted there, despite the enhancement of Z^2 due to the nucleus, the cross sections are already small ($\sim 10^{-10}$ fb) for monopole masses in the range 400 to 1000 GeV, so this work will be focused solely on proton collisions.

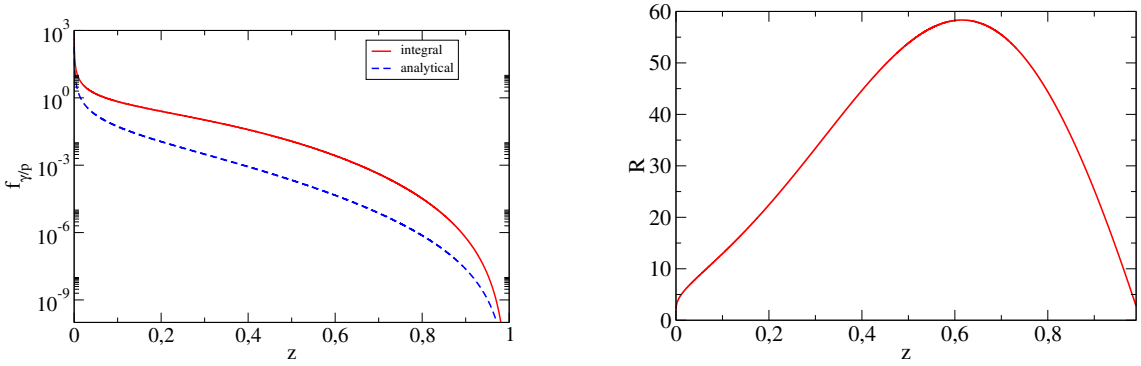

(a) (b) $R = f_{integral}/f_{analytical}$

Figure 4.2: Comparison between the integral and analytical approximation of the elastic photon flux for $\sqrt{s} = 14$ TeV.

According to the formalism of [27], the cross sections for pp collisions can be written in the factorized form, with the cross section for the subprocess of interest and the required photon fluxes and quark distributions. The form of the collisions can be divided in four types (M represents the production of a pair $m\bar{m}$ or a monopolium):

1. Elastic: $p + p \to p + p + 2\gamma \to p + p + M$,

   The factorized cross section will be

$$\sigma_{pp}^{el} = \int_{4m^2/s}^{1} dz_1 \int_{4m^2/sz_1}^{1} dz_2 f_{\gamma/p}^{el}(z_1) f_{\gamma/p}^{el}(z_2) \hat{\sigma}_{\gamma\gamma}(\hat{s} = z_1 z_2 s), \tag{4.18}$$

   with z_i the fraction of the proton energy carried by the photon 1 or 2, and $f_{\gamma/p}^{el}$ the elastic photon flux of the proton, given by (4.15).

2. Semielastic: $p + p \to p + X + 2\gamma \to p + X + M$,

   with X representing an unknown state. The cross section will be

$$\begin{aligned}\sigma_{pp}^{semi}(s) = 2\sum_q \int_{4m^2/s}^{1} dx_1 \int_{4m^2/sx_1}^{1} dz_1 \int_{4m^2/sx_1z_1}^{1} dz_2 \\ \times f_{q/p}(x_1, Q^2) f_{\gamma/q}(z_1) f_{\gamma/p}^{el}(z_2) \hat{\sigma}_{\gamma\gamma}(\hat{s} = x_1 z_1 z_2 s),\end{aligned} \tag{4.19}$$

   with $f_{\gamma/q}$ the equivalent photon spectrum of a quark with charge e_q, given by (4.7). For the structure function $f_{q/p}$, it was used the Cteq6-1L parametrization [56], with scale $Q^2 = \hat{s}/4$.

3. Inelastic: $p + p \to X + X + 2\gamma \to X + X + M$

   The cross section will be

$$\begin{aligned}\sigma_{pp}^{inel}(s) = \sum_{q,q'} \int_{4m^2/s}^{1} dx_1 \int_{4m^2/sx_1}^{1} dx_2 \int_{4m^2/sx_1x_2}^{1} dz_1 \int_{4m^2/sx_1x_2z_2}^{1} dz_2 \\ \times f_{q/p}(x_1, Q^2) f_{q'/p}(x_2, Q^2) f_{\gamma/q}(z_1) f_{\gamma/q'}(z_2) \hat{\sigma}_{\gamma\gamma}(\hat{s} = x_1 x_2 z_1 z_2 s),\end{aligned} \tag{4.20}$$

4. Drell Yan: $p + p \to X + X + q + \bar{q} \to X + X + M$

   The cross section is

$$\sigma_{pp}^{DY}(s) = \sum_q \int_{4m^2/s}^1 dx_1 \int_{4m^2/x_1 s}^1 dx_2 \, f_{q/p}(x_1) f_{\bar{q}/p}(x_2) \hat{\sigma}_{q\bar{q}}(\hat{s} = x_1 x_2), \quad (4.21)$$

   with $f_{q/p}$ given by the Cteq6-1L parametrization [56], again with scale $Q^2 = \hat{s}/4$.

Energy Distribution

The energy distribution of a certain process gives the energy range where it has a higher probability to occur, and is relevant for phenomenological analysis. For the processes considered here, the distribution will be taken about the center of mass energy of the subprocess (photon fusion or Drell Yan) $E_\gamma = \sqrt{\hat{s}}$, which can be related to the velocity β by the expression

$$E_\gamma = \frac{M_{tot}}{\sqrt{1-\beta^2}}, \quad (4.22)$$

where M_{tot} is M or $2m$ for monopolium or monopole pair production, respectively.

To obtain an energy distribution, it is suitable to perform the change of variables as follows:

$$v = z_1 z_2, \;\; w = z_2$$

for elastic collisions,

$$v = z_1 z_2 x_1, \;\; w = z_2 x_1, \;\; u = x_1$$

for semielastic collisions and

$$v = z_1 z_2 x_1 x_2, \;\; w = z_2 x_1 x_2, \;\; u = x_1 x_2, \;\; t = x_2$$

for inelastic collisions.

Fixing the new variable v is equivalent to keep the center of mass energy of the subprocess $E_\gamma = \sqrt{\hat{s}} = \sqrt{vs}$ constant. With the new variables, the integrals (4.18), (4.19) and (4.20) become, respectively,

$$\sigma_{pp}^{el}(s) = \int_{4m^2/s}^1 dv \int_v^1 \frac{dw}{w} \, f_{\gamma/p}^{el}(v/w) f_{\gamma/p}^{el}(w) \hat{\sigma}_{\gamma\gamma}(vs), \quad (4.23)$$

$$\begin{aligned} \sigma_{pp}^{semi}(s) =& 2 \sum_q \int_{4m^2/s}^1 dv \int_v^1 \frac{dw}{w} \int_w^1 \frac{du}{u} \\ & \times f_{q/p}(u, Q^2) f_{\gamma/q}(v/w) f_{\gamma/p}^{el}(w/u) \hat{\sigma}_{\gamma\gamma}(vs), \end{aligned} \quad (4.24)$$

$$\begin{aligned} \sigma_{pp}^{inel}(s) =& \sum_{q,q'} \int_{4m^2/s}^1 dv \int_v^1 \frac{dw}{w} \int_w^1 \frac{du}{u} \int_u^1 \frac{dt}{t} \\ & \times f_{q/p}(u/t, Q^2) f_{q'/p}(t, Q^2) f_{\gamma/q}(v/w) f_{\gamma/q'}(w/u) \hat{\sigma}_{\gamma\gamma}(vs). \end{aligned} \quad (4.25)$$

The distributions will be then

$$\frac{d\sigma_{pp}^{el}}{dE_\gamma}(E_\gamma, s) = \frac{2E_\gamma}{s} \hat{\sigma}_{\gamma\gamma}(\hat{s}) \int_{\hat{s}/s}^1 \frac{dw}{w} \, f_{\gamma/p}^{el}\left(\frac{\hat{s}}{ws}\right) f_{\gamma/p}^{el}(w), \quad (4.26)$$

with the elastic and semielastic of similar form.

4.3 Experimental Search for Magnetic Monopoles

The MoEDAL experiment

The MoEDAL experiment is dedicated to the search of magnetic monopoles among possible others highly ionizing particles produced in the LHC that could indicate some new physics[18]. Highly ionizing particles (HIPs) are characterized by their large electric charge that results in high ionization and stopping power in detectors. The experiment consists in a Magnetic Monopole Trapper (MMT) composed by aluminum trapping detector samples distributed in the forward and lateral regions at the LHCb interaction point. In the last data acquisition[19], the samples were exposed to $4\,\mathrm{fb}^{-1}$ of 13 TeV pp collisions and then scanned with a magnetometer whose response is given in terms of the unitary magnetic charge (1.12). On this set, the presence of a magnetic charge is measured as a persistent current when submitted to a superconducting coil in the magnetometer. From the obtained samples they were able to exclude the presence of magnetic monopoles with charge $|g| > g_o$ with a threshold of $0.4g_o$.

The last results of MoEDAL[19] were the first experimental work to consider the monopole production by photon fusion in addition to the production by Drell Yan, as well as monopoles with spin 0, 1/2 and 1 and magnetic charges up to $5g_o$ including the β dependence. Since no particle was detected, they obtained inferior mass limits for each model of magnetic monopole. The limits of interest for this work are presented in Table 4.1 together with the previous results of the experiment.

Process/Coupling	2019	2018	2017
DY	1320	1110	890
DY (β dep.)	670	850	-
DY + $\gamma\gamma$	2420	-	-
DY + $\gamma\gamma$ (β dep.)	1760	-	-

Table 4.1: Mass limits (in GeV) obtained by MoEDAL [19],[57],[58] for a spin 1/2 monopole with $g = g_o$ at 13 TeV pp collisions.

The ATLAS detector

The search for HIPs, including the magnetic monopole, is also one of the current purposes of the ATLAS detector[28]. The section of the detector dedicated to this search consists of a transition radiation tracker (TRT) composed by straws filled with Xenon (Xe) or Argon (Ar) gas oriented parallel and radially to the beam line, a superconducting solenoid surrounding the TRT and an electromagnetic calorimeter outside the solenoid. The tracking of a HIP starts with an energy deposit greater than 6 keV in Xe or 2 keV in Ar straws. The particles then produce a region of high ionization still in the TRT, leaving a trail of δ radiation (high energetic electrons), and usually stop or slow down in the calorimeter due to their high mass.

The last results of ATLAS[20] contained data from $34.4\,\mathrm{fb}^{-1}$ in 13 TeV pp collision, and no candidate for magnetic monopoles with charge up to $2g_o$ was found. The lower mass limits were then obtained for monopoles with spin 0 and 1/2 and charges g_o and $2g_o$ (without β dependence) produced via the Drell Yan mechanism.

For the monopole considered in this work, the limit was found to be $m < 2370$ GeV, which complements the results obtained by the MoEDAL.

Future Accelerators

Taking these high limits into account, it is very probable that the search for magnetic monopoles will continue in future accelerators with higher collision energies and luminosities. For this reason our simulations are extended to the HE-LHC[30] and FCC[31] colliders, expected to begin their operations after 2035, and to the high luminosity LHC (HL-LHC)[29], which will begin its operations in 2027 with the same energies of the LHC and a higher luminosity.

The main parameters of the pp colliders considered in the calculations are presented in Table 4.2. The luminosity per year refers to the total luminosity of allocated physics time in a year, which corresponds to 160 days for all accelerators.

Parameters	LHC	HL-LHC	HE-LHC	FCC
Beam Energy	14	14	27	100
Peak Luminosity	1	5	16	5-30
Luminosity per year	55	350	500	250-1000

Table 4.2: Main parameters of the LHC, HE-LHC and FCC colliders[30][59]. The beam energy is given in TeV, the peak luminosity in 10^{-5} fb^{-1}/s, and the luminosity per year in fb^{-1}.

Chapter 5

Results and Conclusions

Monopole production

The cross sections for the monopole pair production with $\tilde{\kappa} = 0$, at center of mass energy $\sqrt{s} = 14$ TeV and at future accelerators are presented in Fig. 5.1 and Fig. 5.2. The results corroborate with those in [15], [16] and [21], meaning that the two-photon process has higher cross sections and it is a good candidate for simulations in LHC and new accelerators. For $m \gtrsim 5500$ GeV the Drell Yan cross section overcomes the photon fusion, and this phenomenon also occurs in the HE-LHC and FCC calculations for $m \gtrsim 10$ TeV and $m \gtrsim 40$ TeV, respectively, as shown in Fig. 5.2. However, when considering the luminosities in Table 4.2, the cross sections for these masses are not relevant in any of the accelerators.

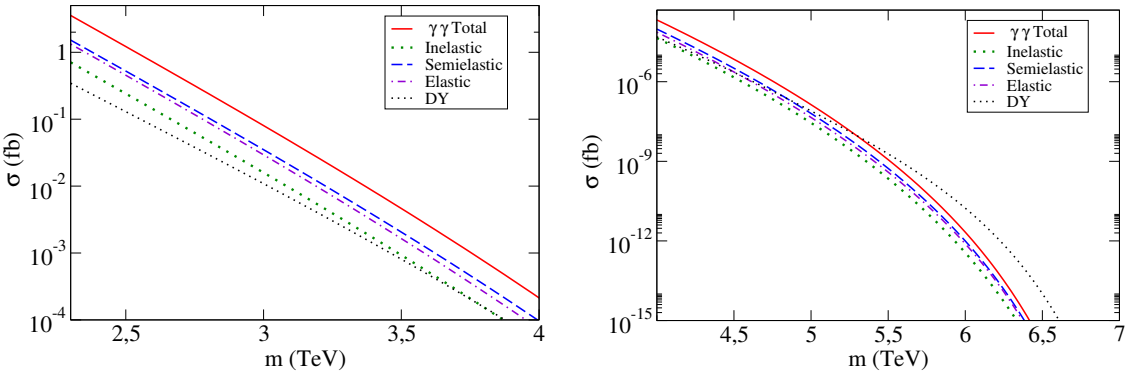

Figure 5.1: Monopole pair production via photon fusion and Drell Yan in pp collisions at $\sqrt{s} = 14$ TeV with $\tilde{\kappa} = 0$.

In Table 5.1, the expected number of events per year for monopole production considering both Drell Yan and photon fusion are displayed. It can be seen that even for the LHC successor, the HL-LHC, monopoles with $m \geq 3$ TeV would probably not produce enough data to be confirmed. With the HE-LHC and FCC, monopoles with masses $m \lesssim 5$ TeV and $m \lesssim 18$ TeV, respectively, would have a higher probability to be detected.

The total cross sections for pair production considering both photon fusion and Drell Yan are compared in Fig. 5.3 for different values of the magnetic moment parameter $\tilde{\kappa}$, again for $\sqrt{s} = 14$ TeV. The results in [21] point out that the cross sections (3.6) and (3.22) for the subprocesses and the total cross sections increase

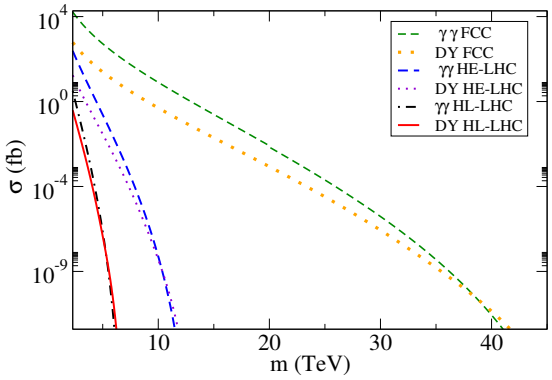

Figure 5.2: Monopole pair production via photon fusion and Drell Yan in pp collisions with $\tilde{\kappa} = 0$.

Mass (TeV)	LHC	HL-LHC	HE-LHC	FCC
3	< 10	< 40	$< 3 \cdot 10^4$	$< 2 \cdot 10^7$
5	$< 2 \cdot 10^{-5}$	$< 8 \cdot 10^{-5}$	< 150	$< 2 \cdot 10^6$
9	0	0	$< 4 \cdot 10^{-4}$	$< 3 \cdot 10^4$
20	0	0	0	< 10
30	0	0	0	$< 2 \cdot 10^{-3}$

Table 5.1: Number of events of monopole production (Drell Yan + photon fusion) per year, for different monopole masses.

with the parameter κ, and the same behavior is achieved for the entire mass range. The cross section for $\tilde{\kappa} = 3$ is up to 10^2 times higher than the one for $\tilde{\kappa} = 0$ only in photon fusion and around 10 times higher in Drell Yan. It can then be concluded that the addition of the magnetic moment parameter, besides providing more applicability to the perturbation methods, can also increase the monopole detection chances.

The results of energy distribution for monopole production are presented in Fig. 5.4 and Fig. 5.5. and follow the same behavior of the cross sections, with higher values for photon fusion compared to Drell Yan and for higher values of $\tilde{\kappa}$. The $\tilde{\kappa} = 3$ distribution for photon fusion is 10^3 times higher than the one for $\tilde{\kappa} = 0$.

Monopolium Production

The results for Monopolium production are in Fig. 5.6 and Fig. 5.7, and it can be seen that the cross section decreases with a lower rate when the monopolium mass is raised, compared to the monopole pair production. The production is also increased for higher values of monopole mass in the entire range, supporting the results in [16], [47] and [55].

Considering a minimum of 1 event per year, for the monopolium production the limits of detection in LHC are $M \lesssim 5$ TeV, for a fixed monopole mass of $m = 3$ TeV. For the HE-LHC and FCC energies and luminosities this limit is close to the maximum possible mass, $M = 6$ TeV. For better estimates of production and detection, it is necessary to analyze the possible decay channels of the monopolium.

The results of energy distribution for monopolium production are presented in

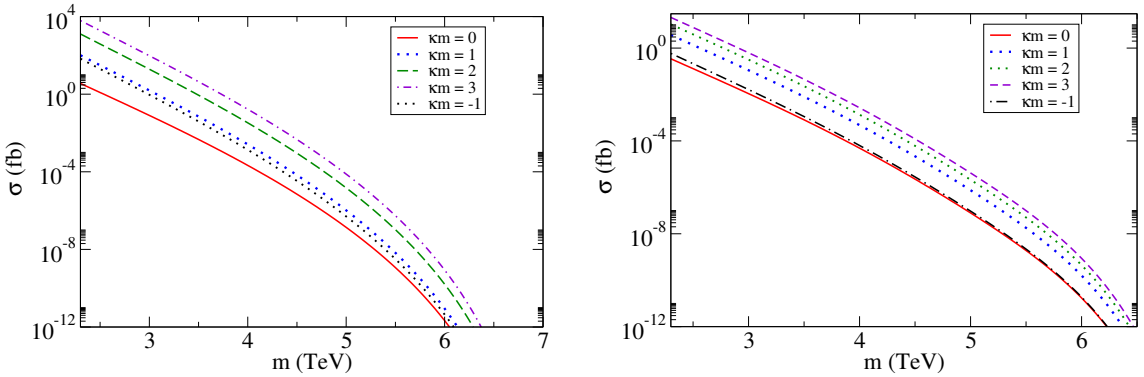

(a) $\gamma\gamma$ (b) DY

Figure 5.3: Monopole pair production via photon fusion and Drell Yan in pp collisions $\sqrt{s} = 14$ TeV for different values of κ.

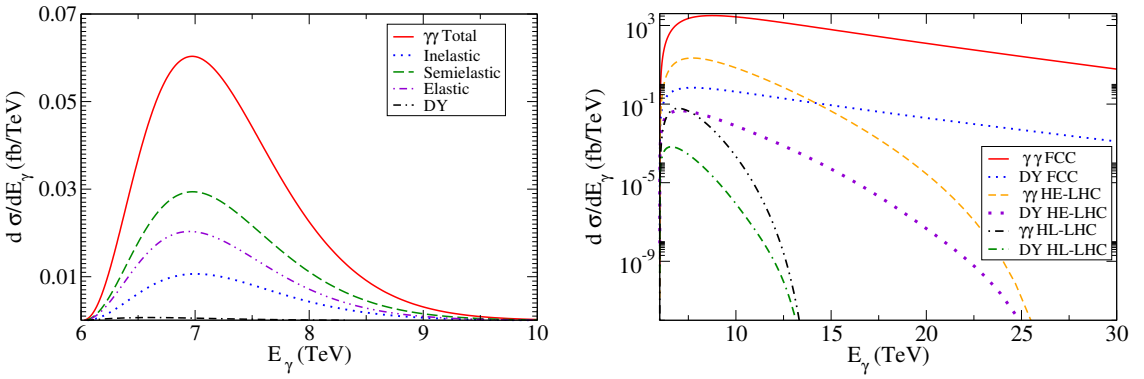

(a) $\sqrt{\hat{s}} = 14$ TeV (b)

Figure 5.4: Energy distribution of monopole pair production with $m = 3$ TeV via photon fusion and Drell Yan in pp collisions with $\tilde{\kappa} = 0$.

Fig. 5.7d. The peak of the distributions occurs right after the energy threshold, as also seen in the distributions for partial cross sections in [16]. The distributions follow the cross sections behavior, having higher values for higher monopole masses as in Fig. 5.6a.

Conclusions

All the estimates made in this work are for an elementary particle with spin 1/2 and undefined mass that carries a magnetic charge. For this model, even if the mass is in the current detectable range, one would still have to deal with the large coupling issue. A way to avoid this limitation is to consider the monopole pair production by the Schwinger mechanism[60]-[62] in strong magnetic fields, such as the ones produced in heavy ion collisions and neutron stars[63]. Other monopole models that are also strong candidates include the GUT [7]-[11] and electroweak monopoles[6]. However, the GUT monopoles have predicted masses around 10^{16} GeV, and the monopole in the electroweak formalism does not have yet a complete description.

If magnetic monopoles do exist and are produced by the processes discussed here, it is reasonable to expect that their experimental evidence may take a while to be

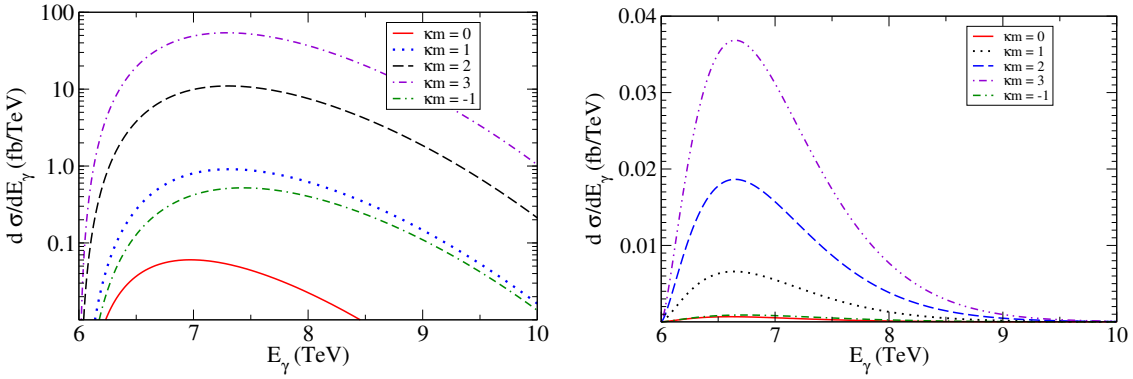

(a) $\gamma\gamma$ (b) DY

Figure 5.5: Energy distribution of monopole pair production with $m = 3$ TeV via photon fusion and Drell Yan in pp collisions $\sqrt{s} = 14$ TeV for different values of $\tilde{\kappa}$.

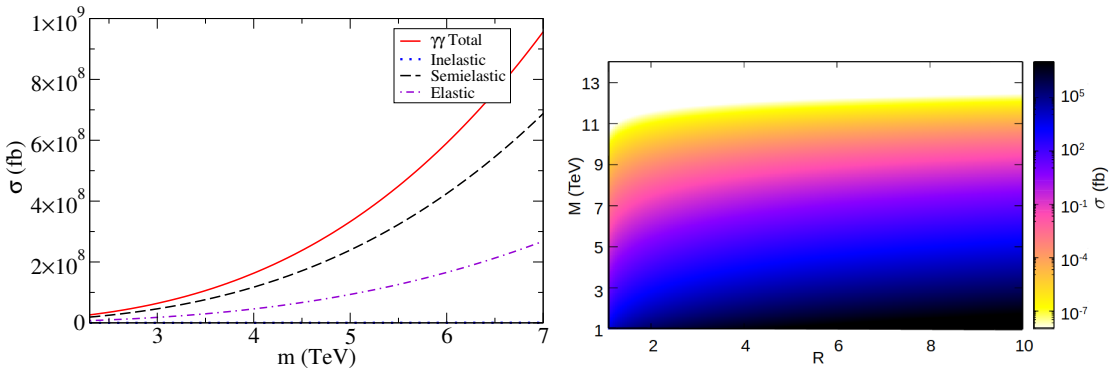

(a) $M = 1$ TeV (b)

Figure 5.6: Monopolium production for fixed (a) and running (b) monopolium masses via photon fusion in pp collisions $\sqrt{s} = 14$ TeV.

obtained. The absence of a well built perturbative theory to study the magnetic monopole in the QED is still one of the greatest difficulties in obtaining new predictions for their interactions. Our results confirm that the production by photon fusion is more relevant in the cross section range that allows detection in LHC and future accelerators. Although also preliminary, the study of the magnetic moment term could lead to more applicability and new results to increase the chances of detection of such particles.

The next steps in the search for magnetic monopoles will depend on future results given by the experiments in accelerators, followed by improvements on the current models. If the lower bounds continue to grow, this may indicate that one has to look for other possible monopole sources. Also, the implementation of other models such as the electroweak monopole in the simulations made in this work are of great interest, since there are very little discussions about their production in present accelerators.

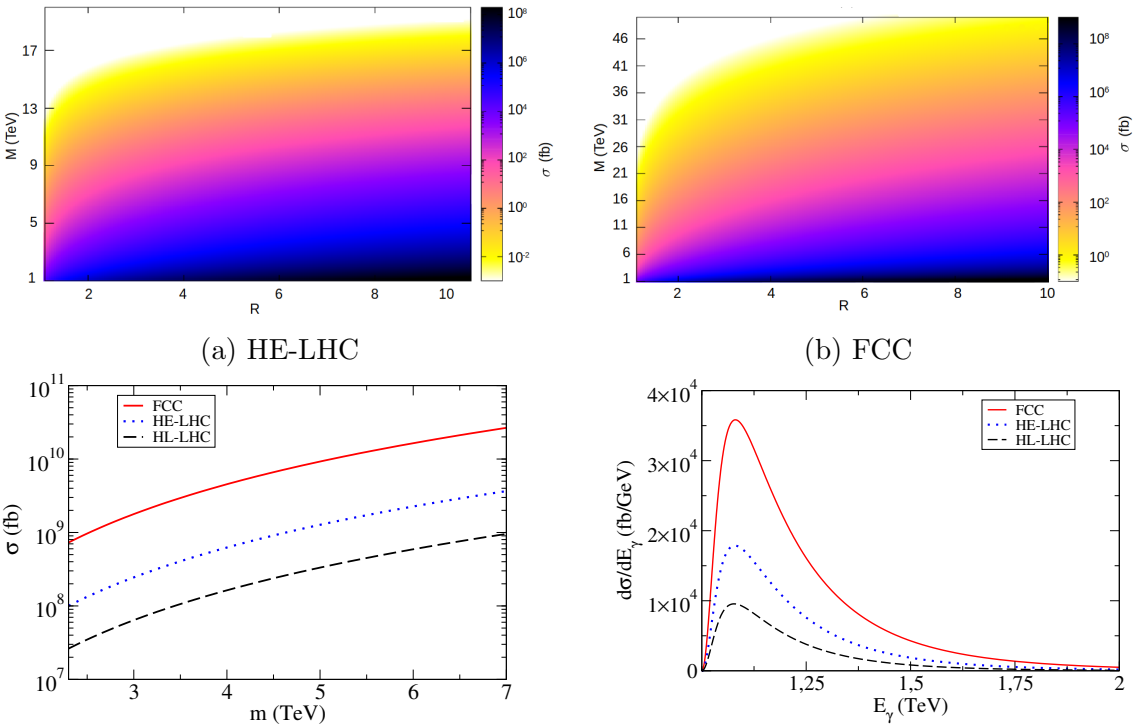

(a) HE-LHC

(b) FCC

(c) $M = 1$ TeV

(d) $m = 3$ TeV, $M = 1$ TeV

Figure 5.7: Monopolium production cross sections and energy distribution for different accelerators

Appendix A

Basic Definitions

Here are some basic definitions and notation used for cross section calculations and along the chapters.

- **Space-time metric**

  A four dimensional position vector x^μ is defined as ($c = 1$)

  $$x^\mu \equiv (t, \mathbf{x}) = (x^0, \mathbf{x}), \tag{A.1}$$

  as well as the velocity, momentum for a particle of mass m and gradient vectors

  $$u^\mu = (\gamma, \gamma\mathbf{u}), \;\; p^\mu = (m, \mathbf{p}), \;\; \partial^\nu = \frac{\partial}{\partial x_\nu} = \left(\frac{\partial}{\partial x_0}, -\nabla\right) \tag{A.2}$$

  respectively, where γ is the Lorentz factor

  $$\gamma = \left(\sqrt{1 - |\mathbf{u}|^2}\right)^{-1} \equiv \left(\sqrt{1 - \beta^2}\right)^{-1}. \tag{A.3}$$

  All the signs follow the convention of the metric tensor

  $$\eta^{\mu\nu} = g^{\mu\nu} = \begin{pmatrix} 1 & 0 & 0 & 0 \\ 0 & -1 & 0 & 0 \\ 0 & 0 & -1 & 0 \\ 0 & 0 & 0 & -1 \end{pmatrix}, \tag{A.4}$$

  which also defines the dot product ($A^\mu = (A^0, \mathbf{A})$):

  $$A_\mu B^\mu = A^0 B^0 - \mathbf{A} \cdot \mathbf{B} \tag{A.5}$$

- **Mandelstam Variables**

  The Mandelstam variables are very useful in scattering theory, as they are defined in terms of the initial and final momenta of particles in a two-particle scattering. The Figure A.1 depicts a general form of this process, where the circle represents all the virtual particles and vertices involved. The Mandelstam variables are then defined as [64]

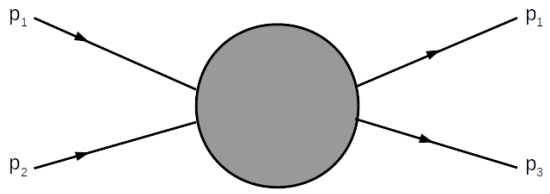

Figure A.1: General process with two initial and final particles.

$$\begin{aligned} s &= (p_1 + p_2)^2 = (p_3 + p_4)^2 \\ t &= (p_3 - p_1)^2 = (p_2 - p_4)^2 \\ u &= (p_3 - p_2)^2 = (p_1 - p_4)^2 \\ s + t + u &= \sum_i m_i^2, \end{aligned} \tag{A.6}$$

where the sum is made over all the initial and final particles.

- **Annihilation and Creation Operators** The creation and annihilation operators are useful when dealing with multiple particle states, for they are defined as operators that add or remove a particle from a given state, respectively. If a state Φ is composed by N particles $q_1, q_2, \ldots, q_N$, the creation operator can be defined by

$$a^\dagger(q)\Phi_{q_1,q_2,\ldots,q_N} = \Phi_{q,q_1,q_2,\ldots,q_N}, \tag{A.7}$$

where q represents the added particle. The state $\Phi_{q_1,q_2,\ldots,q_N}$ can also be defined in terms of the vacuum state Φ_0 by the successive multiplication of creation operators

$$a^\dagger(q_1)a^\dagger(q_1)\ldots a^\dagger(q_N)\Phi_0 = \Phi_{q_1,q_2,\ldots,q_N}. \tag{A.8}$$

The annihilation operator is the adjoint of $a^\dagger(q)$ and can be defined as the operator that annihilates the vacuum state,

$$a(q)\Phi_0 = 0. \tag{A.9}$$

The action of $a(q)$ over a general multiparticle state will vary if the state is composed by fermions (spin half particles), bosons (spin integer particles) or a combination of both. For the particular cases where particles are all fermions or all bosons, the operator will act as

$$a(q)\Phi_{q_1,q_2,\ldots,q_N} = \sum_{r=1}^{N}(\pm)^{r+1}\delta(q - q_r)\Phi_{q_1,\ldots,q_{r-1},q_{r+1},\ldots,q_N}, \tag{A.10}$$

where we use + for bosons and − for fermions. Multiplying a to the left of (A.8) and $a\dagger$ to the left of (A.10), we can derive the commutation relations for the operators

$$[a(q')a^\dagger(q) \mp a^\dagger(q)a(q')]\Phi_{q_1,q_2,\ldots,q_N} = \delta(q' - q)\Phi_{q_1,q_2,\ldots,q_N}, \tag{A.11}$$

where the upper sign − is for bosons and the lower sign + for fermions.

- **Dirac Matrices** The Dirac matrices, or gamma matrices, γ^μ are hermitian and satisfy the anticommutation relations

$$\{\gamma^\mu, \gamma^\nu\} = \gamma^\mu\gamma^\nu + \gamma^\nu\gamma^\mu = 2g^{\mu\nu}. \tag{A.12}$$

They fulfill many trace identities, some of them very handy in cross section calculation, such as

1. $\mathrm{Tr}\,(\gamma^\mu) = \mathrm{Tr}\,(\gamma^\mu\gamma^\nu\gamma^\alpha) = \mathrm{Tr}\,(\gamma^\mu\gamma^\nu\dots) = 0$ for any product of an odd number of gamma matrices
2. $\mathrm{Tr}\,(\gamma^\mu\gamma^\nu) = 4g^{\mu\nu}$
3. $\mathrm{Tr}\,(\gamma^\mu\gamma^\nu\gamma^\alpha\gamma^\beta) = 4(g^{\mu\nu}g^{\alpha\beta} - g^{\mu\alpha}g^{\nu\beta} + g^{\mu\beta}g^{\nu\alpha})$.
4. For n even
$$\mathrm{Tr}\,(\gamma^{\nu_1}\gamma^{\nu_2}\dots\gamma^{\nu_n}) = \sum_{k=2}^{n}(-1)^k g^{\nu_1\nu_k}\mathrm{Tr}\,(\gamma^{\nu_2}\dots\cancel{\gamma^{\nu_k}}\dots\gamma^{\nu_n})$$
5. $\mathrm{Tr}\,(\gamma^\mu\gamma^\nu\dots\gamma^\alpha\gamma^\beta) = \mathrm{Tr}\,(\gamma^\beta\gamma^\alpha\dots\gamma^\nu\gamma^\mu)$ for any product of gamma matrices.

The slash notation for a four vector A^μ is defined by

$$\cancel{A} \equiv \gamma^\mu A_\mu, \tag{A.13}$$

and has some similar trace identities:

1. $\mathrm{Tr}\,(\cancel{A}\cancel{B}) = 4A_\mu B^\mu$
2. $\mathrm{Tr}\,(\cancel{A}\cancel{B}\cancel{C}\cancel{D}) = 4[(A_\mu B^\mu)(C_\mu D^\mu) - (A_\mu C^\mu)(B_\mu D^\mu) + (A_\mu D^\mu)(B_\mu C^\mu)]$.

Another notation involving the Dirac matrices, sometimes called of adjoint, is

$$\bar{\psi} = \psi^\dagger\gamma^0, \tag{A.14}$$

where ψ is a Dirac spinor or field (column matrix with four components).

The angular differential cross section for two initial particles, in the center of mass frame, can be defined as

$$\frac{d\sigma}{d\Omega} = \frac{1}{64\pi^2 s}\frac{|\mathbf{p}_1|}{|\mathbf{q}_1|}|\bar{M}|^2, \tag{A.15}$$

with $\mathbf{p}_1$ and $\mathbf{q}_1$ as in Figure B.2 and s representing the total energy squared, as part of the the Mandelstam variables:

where the sum is over all the particles involved in the process. $|\bar{M}|^2$ is the squared total amplitude, averaged over initial polarization states (or spin if the initial particles are fermions) and summed over the final spin states (or polarization if the final particles are photons). To obtain this last term, it is necessary to know the sum over photon polarization states

$$\sum_\lambda \epsilon^\mu_\lambda \epsilon^{\nu *}_\lambda = -g^{\mu\nu}, \tag{A.16}$$

and the spinor sum rules over spin and polarization states

$$\sum_s u_{s\alpha}(\mathbf{p}_1)\bar{u}_{s\beta}(\mathbf{p}_1) = (\not{p}_1 + m)_{\alpha\beta}, \quad \sum_r v_{r\alpha}(\mathbf{p}_2)\bar{v}_{r\beta}(\mathbf{p}_2) = (\not{p}_2 - m)_{\alpha\beta}. \tag{A.17}$$

Appendix B

Cross Sections

B.1 Lepton pair production by Drell Yan

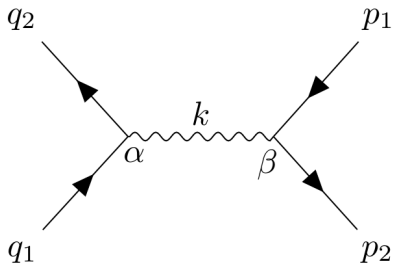

Figure B.1: Lepton production by Drell Yan

To obtain the Drell Yan cross section for lepton production at tree-level, we consider the Feynman graph B.1. To write the amplitude we use the quarks, leptons and photon momenta and the vertexes labels α and β

$$\mathscr{M}_{DY} = u_r(\mathbf{q}_1)(iq_q\gamma^\alpha)\bar{v}_{r'}(\mathbf{q}_2)\frac{-i\eta_{\alpha\beta}}{k^2}\bar{u}_s(\mathbf{p}_1)(iq_l\gamma^\beta)v_{s'}(\mathbf{p}_2), \tag{B.1}$$

where q_q and q_l are the quark and lepton charges, respectively. Squaring and summing over the spin indices, we get

$$\begin{aligned}|\mathscr{M}_{DY}|^2 = \sum_{r,r'}\sum_{s,s'}\frac{1}{4}\frac{1}{3}&\left[u_r(iq_q\gamma^\alpha)\bar{v}_{r'}\frac{-i\eta_{\alpha\beta}}{k^2}\bar{u}_s(iq_l\gamma^\beta)v_{s'}\right]\\ &\times\left[\bar{v}_{s'}(-iq_l\gamma^{\beta'})u_s\frac{i\eta_{\alpha'\beta'}}{k^2}v_{r'}(-iq_q\gamma^{\alpha'}\bar{u}_r)\right],\end{aligned} \tag{B.2}$$

where the momentum dependence of u and v are dropped off for a cleaner notation, and the factors $1/4$ and $1/3$ correspond to the averaging over spinor and color states of the quarks, respectively. The next step is to write each product between a vector and a matrix by their components

$$\begin{aligned}|\mathscr{M}_{DY}|^2 = \sum_{r,r'}\sum_{s,s'}\frac{q_q^2q_l^2}{12}&\left[u_{r\gamma}[\gamma^\alpha]_{\gamma\delta}\bar{v}_{r'\delta}\frac{\eta_{\alpha\beta}}{k^2}\bar{u}_{s\epsilon}[\gamma^\beta]_{\epsilon\pi}v_{s'\pi}\right]\\ &\times\left[\bar{v}_{s'\rho}[\gamma^{\beta'}]_{\rho\sigma}u_{s\sigma}\frac{\eta_{\alpha'\beta'}}{k^2}v_{r'\lambda}[\gamma^{\alpha'}]_{\lambda\xi}\bar{u}_{r\xi}\right].\end{aligned} \tag{B.3}$$

Now we sum over the spin indices

$$|\mathscr{M}_{DY}|^2 = \frac{q_q^2 q_l^2}{12}\frac{\eta_{\alpha\beta}}{k^2}\frac{\eta_{\alpha'\beta'}}{k^2}\Big[(\not{q}_1 + m_q)_{\gamma\xi}[\gamma^\alpha]_{\gamma\delta}(\not{q}_2 - m_q)_{\delta\lambda}(\not{p}_1 + m_l)_{\epsilon\sigma} \times[\gamma^\beta]_{\epsilon\pi}(\not{p}_2 - m_l)_{\pi\rho}[\gamma^{\beta'}]_{\rho\sigma}[\gamma^{\alpha'}]_{\lambda\xi}\Big], \tag{B.4}$$

$$\begin{aligned}\rightarrow |\mathscr{M}_{DY}|^2 =& \frac{q_q^2 q_l^2}{12}\frac{\eta_{\alpha\beta}}{k^2}\frac{\eta_{\alpha'\beta'}}{k^2}\mathrm{Tr}\left[(\not{q}_1 + m_q)\gamma^\alpha(\not{q}_2 - m_q)\gamma^{\alpha'}\right] \\ &\times \mathrm{Tr}\left[(\not{p}_1 + m_l)\gamma^\beta(\not{p}_2 - m_l)\gamma^{\beta'}\right].\end{aligned} \tag{B.5}$$

Calculating the traces with the identities given in Appendix A and summing the remaining indices with the metrics $\eta_{\alpha\beta}$ and $\eta_{\alpha'\beta'}$, we get

$$\begin{aligned}|\mathscr{M}_{DY}|^2 = \frac{8q_q^2 q_l^2}{3k^4}\big[&(q_1\cdot p_1)(q_2\cdot p_2) + (q_1\cdot p_2)(q_2\cdot p_1) \\ &+ m_l^2(q_1\cdot q_2) + m_q^2(p_1\cdot p_2) + 2m_l^2 m_q^2\big].\end{aligned} \tag{B.6}$$

Since we are working in the center of mass frame, the total energy of each lepton will be equal to each quark, and we can set $E_l = E_q \equiv E$ to calculate the scalar products. In the notation used here, the momentum is given in the form $p = (E, \vec{p})$, and the scalar products will be

$$\begin{aligned}q_1\cdot p_1 &= E_q E_l - \mathbf{q}_1\cdot\mathbf{p}_1 = E^2 - qp\cos\theta = q_2\cdot p_2,\\ q_1\cdot p_2 &= E^2 + qp\cos\theta = q_2\cdot p_1\\ q_1\cdot q_2 &= E^2 + q^2\\ p_1\cdot p_2 &= E^2 + p^2,\end{aligned} \tag{B.7}$$

where $p = |\mathbf{p}_1| = |\mathbf{p}_2|$, $q = |\mathbf{q}_1| = |\mathbf{q}_2|$ and θ is the angle between the leptons and quarks momenta. The photon momentum k can be written in terms of the total energy, using momentum conservation at the vertexes

$$k^2 = (q_1 + q_2)^2 = (p_1 + p_2)^2 = 4E^2 \tag{B.8}$$

and we can then write the momenta q and p in terms of the boosts

$$\beta_{q(l)} = \frac{|\mathbf{q}(\mathbf{p})|}{E} \tag{B.9}$$

to get

$$|\mathscr{M}_{DY}|^2 = \frac{q_q^2 q_l^2}{3}\Big[3 - \beta_q^2 - \beta_l^2 + \beta_l^2\beta_q^2\cos^2\theta\Big]. \tag{B.10}$$

The cross section will be

$$\begin{aligned}\frac{d\hat{\sigma}}{d\Omega} =& \frac{1}{64\pi^2\hat{s}}\frac{p}{q}\frac{q_q^2 q_l^2}{3}\Big[3 - \beta_q^2 - \beta_l^2 + \beta_l^2\beta_q^2\cos^2\theta\Big]\\ =& \frac{\alpha_q\alpha_l}{12\hat{s}}\frac{\beta_l}{\beta_q}\Big[3 - \beta_q^2 - \beta_l^2 + \beta_l^2\beta_q^2\cos^2\theta\Big],\end{aligned} \tag{B.11}$$

where $\alpha_{q(l)} = \frac{q_q(q_l)^2}{4\pi}$. Integrating over all solid angles, we get the final cross section

$$\sigma(\hat{s}) = \frac{\pi\alpha_q\alpha_l}{9\hat{s}}\frac{\beta_l}{\beta_q}\Big[9 - 3(\beta_q^2 + \beta_l^2) + \beta_l^2\beta_q^2\Big]. \tag{B.12}$$

B.2 Lepton pair production by photon fusion

To obtain the total cross section for a lepton pair production with charge q_l, we have to sum over the amplitudes of the t-channel and u-channel, depicted in Fig. B.2. We proceed the calculation for a general lepton with charge q.

(a) t-channel. (b) u-channel.

Figure B.2: Spin 1/2 electron-positron (or monopole-antimonopole) pair production by photon fusion

The total first order amplitude will be

$$M_{\gamma\gamma} = M_t + M_u, \tag{B.13}$$

with

$$M_t = \epsilon_{\lambda\mu}(\mathbf{q}_1)\bar{u}_s(\mathbf{p}_1)(iq_l\gamma^\mu)i\left(\frac{\not{k}+m}{k^2-m^2}\right)(iq_l\gamma^\nu)v_r(\mathbf{p}_2)\epsilon_{\lambda'\nu}(\mathbf{q}_2) \text{ and} \tag{B.14}$$

$$M_u = \epsilon_{\lambda'\mu}(\mathbf{q}_2)\bar{u}_s(\mathbf{p}_1)(iq_l\gamma^\mu)i\left(\frac{\tilde{\not{k}}+m}{\tilde{k}^2-m^2}\right)(iq_l\gamma^\nu)v_r(\mathbf{p}_2)\epsilon_{\lambda\nu}(\mathbf{q}_1). \tag{B.15}$$

The squared averaged amplitude will be

$$\begin{aligned}
|\bar{M}_{\gamma\gamma}|^2 =& \frac{1}{4}\sum_{\lambda,\lambda'}\sum_{r,s}[M_tM_t^* + M_uM_u^* + M_tM_u^* + M_uM_t^*] \\
=& \frac{1}{4}\sum_{\lambda,\lambda'}\epsilon^{*\nu'}_{\lambda'}\epsilon^{\mu}_{\lambda}\epsilon^{\nu}_{\lambda'}\epsilon^{*\mu'}_{\lambda}q_l^4\sum_{r,s}\left[\bar{u}_s\gamma_\mu\left(\frac{\not{k}+m}{k^2-m^2}\right)\gamma_\nu v_r + \bar{u}_s\gamma_\nu\left(\frac{\tilde{\not{k}}+m}{\tilde{k}^2-m^2}\right)\gamma_\mu v_r\right] \\
&\times\left[\bar{v}_r\gamma_{\nu'}\left(\frac{\not{k}+m}{k^2-m^2}\right)\gamma_{\mu'}u_s + \bar{v}_r\gamma_{\mu'}\left(\frac{\tilde{\not{k}}+m}{\tilde{k}^2-m^2}\right)\gamma_{\nu'}u_s\right] \\
=& \frac{q_l^4}{4}g^{\mu\mu'}g^{\nu\nu'}\sum_{r,s}\left[\bar{u}_{s\alpha}\left(\gamma_\mu\left(\frac{\not{k}+m}{k^2-m^2}\right)\gamma_\nu\right)_{\alpha\beta}v_{r\beta} + \bar{u}_{s\delta}\left(\gamma_\nu\left(\frac{\tilde{\not{k}}+m}{\tilde{k}^2-m^2}\right)\gamma_\mu\right)_{\delta\rho}v_{r\rho}\right] \\
&\times\left[\bar{v}_{r\sigma}\left(\gamma_{\nu'}\left(\frac{\not{k}+m}{k^2-m^2}\right)\gamma_{\mu'}\right)_{\sigma\epsilon}u_{s\epsilon} + \bar{v}_{r\kappa}\left(\gamma_{\mu'}\left(\frac{\tilde{\not{k}}+m}{\tilde{k}^2-m^2}\right)\gamma_{\nu'}\right)_{\kappa\pi}u_{s\pi}\right].
\end{aligned} \tag{B.16}$$

In the last step, the indices α, β, $\delta\ldots$ are written explicitly to indicate the product between the spinors and matrices, using the Einstein summation convention.

Denoting each matrix element by $\Gamma_{\mu\nu}$ and summing over r and s,

$$\begin{aligned}
|\bar{M}_{\gamma\gamma}|^2 =& \frac{q_l^4}{4} g^{\mu\mu'} g^{\nu\nu'} \left[\Gamma_{\alpha\beta}\Gamma_{\sigma\epsilon}(\not{p}_1 + m)_{\epsilon\alpha}(\not{p}_2 - m)_{\beta\sigma} + \Gamma_{\alpha\beta}\Gamma_{\kappa\pi}(\not{p}_1 + m)_{\pi\alpha}(\not{p}_2 - m)_{\beta\kappa}\right. \\
&\left. + \Gamma_{\delta\rho}\Gamma_{\sigma\epsilon}(\not{p}_1 + m)_{\epsilon\delta}(\not{p}_2 - m)_{\rho\sigma} + \Gamma_{\delta\rho}\Gamma_{\kappa\pi}(\not{p}_1 + m)_{\pi\delta}(\not{p}_2 - m)_{\rho\kappa}\right] \\
=& \frac{q_l^4}{4} g^{\mu\mu'} g^{\nu\nu'} \mathrm{Tr}\left[(\not{p}_1 + m)\gamma_\mu \left(\frac{\not{k} + m}{k^2 - m^2}\right)\gamma_\nu(\not{p}_2 - m)\gamma_{\nu'}\left(\frac{\not{k} + m}{k^2 - m^2}\right)\gamma_{\mu'}\right. \\
&+ (\not{p}_1 + m)\gamma_\mu \left(\frac{\not{k} + m}{k^2 - m^2}\right)\gamma_\nu(\not{p}_2 - m)\gamma_{\mu'}\left(\frac{\tilde{\not{k}} + m}{\tilde{k}^2 - m^2}\right)\gamma_{\nu'} \\
&+ (\not{p}_1 + m)\gamma_\nu \left(\frac{\tilde{\not{k}} + m}{\tilde{k}^2 - m^2}\right)\gamma_\mu(\not{p}_2 - m)\gamma_{\nu'}\left(\frac{\not{k} + m}{k^2 - m^2}\right)\gamma_{\mu'} \\
&\left. + (\not{p}_1 + m)\gamma_\nu \left(\frac{\tilde{\not{k}} + m}{\tilde{k}^2 - m^2}\right)\gamma_\mu(\not{p}_2 - m)\gamma_{\mu'}\left(\frac{\tilde{\not{k}} + m}{\tilde{k}^2 - m^2}\right)\gamma_{\nu'}\right].
\end{aligned} \tag{B.17}$$

The traces can be evaluated with the properties given in Appendix A, and the result will be in terms of scalar products between the momenta. To write the amplitude in the usual way, it is necessary to use energy and momentum conservation in each vertex:

$$q_1 + k = p_1 \text{ and } q_2 - k = p_2 \tag{B.18}$$

for the u-channel diagram and

$$q_1 - \tilde{k} = p_2 \text{ and } q_2 + \tilde{k} + p_1 \tag{B.19}$$

for the t-channel diagram and write the scalar products that will appear after the calculation of the traces

$$\begin{aligned}
q_1 \cdot p_1 &= E^2 - qp\cos\theta = q_2 \cdot p_1 \\
q_1 \cdot p_2 &= E^2 + qp\cos\theta = q_2 \cdot p_2 \\
q_2 \cdot q_1 &= E^2 - q^2 = 0 \\
p_1 \cdot p_2 &= E^2 + p^2,
\end{aligned} \tag{B.20}$$

where again E is the center of mass energy, $p = \mathbf{p}$ and $q = \mathbf{q}$ are the three momentum module of $p_{1,2}$ and $q_{1,2}$, respectively. Using the definition of β (B.9) and remembering that $\beta_{photon} = 1$, the amplitude will be given by

$$|\bar{\mathscr{M}}_{\gamma\gamma}|^2 = \frac{q_l^4}{4(1 - \beta^2\cos^2\theta)^2}[-2\beta^4 + 2\beta^2 - \beta^4\cos^4\theta + 2\beta^4\cos^2\theta - 2\beta^2\cos^2\theta + 1] \tag{B.21}$$

and the cross section can finally be written

$$\frac{d\hat{\sigma}}{d\Omega} = \frac{\alpha_l^2\beta}{\hat{s}(1 - \beta^2\cos^2\theta)^2}[-2\beta^4 + 2\beta^2 - \beta^4\cos^4\theta + 2\beta^4\cos^2\theta - 2\beta^2\cos^2\theta + 1]. \tag{B.22}$$

Integrating over the solid angle we get

$$\hat{\sigma}_{\gamma\gamma\to l\bar{l}}(\hat{s}) = \frac{4\pi\alpha_l^2\beta}{\hat{s}}\left[\frac{3 - \beta^4}{2\beta}\ln\frac{1 + \beta}{1 - \beta} - (2 - \beta^2)\right]. \tag{B.23}$$

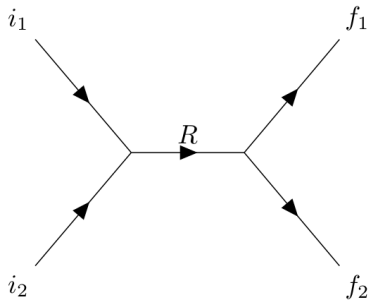

Figure B.3: Production and decay of a resonant state R

B.3 Resonance Production

In a resonance production, the total decay rate can be written in terms of the lifetime τ and the decay rates of each possible final state Γ_f of the particle[65]

$$\Gamma = \frac{1}{\tau} = \sum_f \Gamma_f. \tag{B.24}$$

To write the production cross section of a resonance, we first define $\psi_1(\mathbf{x})$ and $\psi_0(\mathbf{x})$ as the initial and resonance state, respectively, and $\psi_n(\mathbf{x})$ $(n > 1)$ the final states of the possible decay channels, respecting the orthonormality condition

$$\int \psi_n(x)\psi_m^*(x)\, dx = \delta_{mn}. \tag{B.25}$$

The total wave function can then be written as a linear superposition

$$\psi(\mathbf{x}, t) = \sum_{n=0}^{\infty} a_n(t)\mathrm{e}^{-iE_n t}\psi_n(\mathbf{x}), \tag{B.26}$$

where

$$E_n \equiv H_{nn} = \int \psi_n^*(\mathbf{x}) H \psi_n(\mathbf{x})\, d\mathbf{x} \tag{B.27}$$

and the boundary conditions are $a_1(0) = 1$, $a_n(0) = 0$ $(n \neq 1)$. Discarding any spin dependence, we can replace (B.26) into the Schrödinger equation and use the orthonormality condition (B.25) to get the time dependence of $a_n(t)$

$$\frac{da_n(t)}{dt} = -i \sum_{m \neq n} H_{nm}\mathrm{e}^{-i(E_m - E_n)t} a_m(t). \tag{B.28}$$

In first order in H_{nm}, the expression for $a_0(t)$ can be written as[65]

$$\frac{da_0(t)}{dt} = -iH_{01}\mathrm{e}^{-i(E_1 - E_0)t} - \left(\frac{\Gamma}{2}\right) a_0(t), \tag{B.29}$$

where the second term is added to take into account the additional power of H_{0n} (which can involve many final states n) that is ignored if we only consider the dependence in H_{01}. The equation can then be solved to give, for $t \gg 1/\Gamma$,

$$a_0(t) = \frac{H_{01}\mathrm{e}^{-i(E_1 - E_0)t}}{E_1 - E_0 + i\Gamma/2}. \tag{B.30}$$

The total decay rate can be written as

$$W = \Gamma |a_0(t)|^2 = \frac{|H_{01}|^2 \Gamma}{(E_1 - E_0)^2 + \Gamma^2/4}, \tag{B.31}$$

and the cross section is given by

$$\sigma = \frac{V}{v_i} W = \frac{\pi}{q_i^2} \frac{\Gamma_i \Gamma}{(E_1 - E_0)^2 + \Gamma^2/4}, \tag{B.32}$$

where Γ_i is the decay width of the resonance into the initial state, given by

$$\Gamma_i = \frac{V}{\pi} \frac{q_i^2}{v_i} |H_{10}|^2, \tag{B.33}$$

with v_i the relative velocity between the particles in the initial state and q_i their initial momentum. In the center of mass frame, $E_0^2 = M^2$ (mass of the resonance) and for the cases where $\Gamma^2 \ll E_0^2$ we can set the initial energy $E_1 \equiv E$ to write the usual form of (B.32)

$$\sigma(E) = \frac{4\pi}{E^2} \frac{M^2 \Gamma_i \Gamma}{(E^2 - M^2)^2 + M^2 \Gamma^2}. \tag{B.34}$$

Bibliography

[1] P. A. M. Dirac, Proc. Roy. Soc. Lon. A **133**, 60 (1931).

[2] P. A. M. Dirac, Phys. Rev. **74**, 817 (1948).

[3] M. J. Mulhearn, *A Direct Search for Dirac Magnetic Monopoles*, Thesis Fermilab (2004).

[4] CDF Collaboration, Phys. Rev. Lett 96, 201801 (2006).

[5] J. S. Schwinger, Science **165**, 757 (1969).

[6] Y. M. Cho and D. Maison, Phys. Lett. B **391**, 360 (1997).

[7] G. 't Hooft, Nucl. Phys. **B** 79: 276-284 (1974).

[8] A. M. Polyakov, JETP Lett. **20**, 194 (1974); A. M. Polyakov, Pisma Zh. Eksp. Teor. Fiz. **20**, 430 (1974).

[9] Y. Nambu, Phys. Rev. D, **10**, 4262 (1974).

[10] B. Julia and A. Zee, Phys. Rev. D **11**, 2227 (1975).

[11] T. T. Wu and C. N. Yang, Phys. Rev. D **12**, 3843 (1975).

[12] C. T. Hill, Nucl. Phys. B **224**, 469 (1983).

[13] M. Eto, Y. Hamada, M. Kurachi and M. Nitta, JHEP **07**, 004 (2020).

[14] G. R. Kalbfleisch et al., Phys. Rev. Lett **85**, 5292 (2000).

[15] T. Dougall and S. D. Wick, Eur. Phys. J. A **39**, 213 (2009); T. Dougall, *Monopole pair production via photon fusion*, Thesis Southern Methodist University, December 9 (2006).

[16] L. N. Epele, H. Fanchiotti, C. A. G. Canal, V. A. Mitsou and V. Vento, Eur. Phys. J. Plus **127**, 60 (2012).

[17] L. N. Epele, H. Fanchiotti, C. A. G. Canal, V. A. Mitsou and V. Vento, [arXiv:1104.0218 [hep-ph]].

[18] MoEDAL web page: http://moedal.web.cern.ch/ ; B. Acharya *et al* (MoEDAL Collaboration), Int. J. Mod. Phys. A **29**, 1430050 (2014).

[19] B. Acharya *et al.* (MoEDAL Collaboration), Phys. Rev. Lett. **123**, 021802 (2019).

[20] G. Aad *et al.* (ATLAS Collaboration), Phys. Rev. Lett. **124**, 031802 (2020).

[21] S. Baines, N. E. Mavromatos, V. A. Mitsou, J. L. Pinfold and A. Santra, Eur. Phys. J. C **78**, no. 11, 966 (2018); Erratum: [Eur. Phys. J. C **79**, no. 2, 166 (2019)]

[22] V. Budnev, I. Ginzburg, G. Meledin and V. Serbo, Phys. Rept. **15**, 181 (1975).

[23] J. F. Gunion, H. Haber, G. L. Kane and S. Dawson, *The Higgs Hunter's Guide*, Addison-Wesley (1990).

[24] M. B. Gay Ducati and G. G. Silveira, Phys. Rev. D **82**, 073004 (2010).

[25] T. D. Lee, Phys. Rev. D **8**, 1226 (1973); H. Georgi, Hadronic J. **1**, 155 (1978).

[26] S.D. Drell and T.M. Yan, Phys. Rev. Lett. **25**, 316 (1970).

[27] M. Drees, R. M. Godbole, M. Nowakowski and S. D. Rindani, Phys. Rev. D **50**, 2335 (1994).

[28] ATLAS Collaboration, The ATLAS experiment at the CERN Large Hadron Collider, J. Instrum. **3**, S08003 (2008).

[29] The HiLumi Collaboration, Report No. CERN-ACC-2014-0300 (2014).

[30] A. Abada *et al* (FCC collaboration), Collider. Eur. Phys. J. Spec. Top. **228**, 1109–1382 (2019).

[31] Abada, A. *et al* (FCC collaboration), Eur. Phys. J. C **79**, 474 (2019).

[32] B. M. Carlos and M. B. Gay Ducati, [arXiv:2010.03616 [hep-ph]](Submitted to Phy. Rev. D) (2020).

[33] M. B. Gay Ducati and B. M. Carlos, Pos(ICHEP2020)245.

[34] Y. M. Shnir, *Magnetic Monopoles*, Springer (2005).

[35] D.G. Boulware et al, Phys. Rev. D **14**, 2708 (1976).

[36] J. Schwinger, Phys. Rev. **144**, 1087 (1966).

[37] N.F. Ramsey, Phys. Rev. **109**, 225 (1958).

[38] Ya. Shnir, E.A. Tolkachev and L.M. Tomilchik, Int. J. Mod. Phys. **A7**, 3747 (1992).

[39] J. Schwinger, K. A. Milton, W. Tsai, L. L. DeRaad Jr. and D. C. Clark, Annals of Phys. **101**, 451 (1976).

[40] Y. Kurochkin, I. Satsunkevich, D. Shoukavy, N. Rusakovich and Y. Kulchitsky, Mod. Phys. Lett. A **21**, 2873 (2006).

[41] S. Weinberg, *The Quantum Theory of Fields* (v. 1. Foundations), Cambridge University (1996).

[42] F. Mandl and G. Shaw, *Quantum Field Theory*, John Wiley and Sons (1984).

[43] J. Alwall et al., JHEP **1407**, 079 (2014).

[44] H. Fanchiotti, C. A. García Canal and V. Vento, https://www.overleaf.com/project/5da65ca647765f00017057f9Int. J. Mod. Phys. A **32**, 1750202 (2017).

[45] L. I. Schiff, Phys. Rev. **160**, 1257 (1967).

[46] L. N. Epele, H. Fanchiotti, C. A. Garcia Canal and V. Vento, Eur. Phys. J. C **56**, 87 (2008).

[47] L. N. Epele, H. Fanchiotti, C. A. G. Canal and V. Vento, Eur. Phys. J. C **62**, 587 (2009).

[48] E. J. Williams, Phys. Rev. 45 (1934) 729(L); C. F. Weizsaecker, Z.Phys. **88**, 612 (1934).

[49] J. D. Jackson, *Classical Electrodynamics*, John Wiley and Sons (1962).

[50] F. Halzen and A. D. Martin, *Quarks and Leptons: An Introductory Course in Modern Particle Physics*, John Wiley (1984).

[51] V. M. Budnev, I. F. Ginzburg, G. V. Meledin, V. G. Serbo, Phys. Rept. **15**, 181 (1974).

[52] B.A. Kniehl, Phys. Lett. B **254**, 267 (1991).

[53] M. Drees and D. Zeppenfeld, Phys. Rev. D **39**, 2536 (1989).

[54] Y. V. Kovchegov and E. M. Levin, *Quantum Chromodynamics at High Energy*, Cambridge Monographs on Particle Physics, Vol 33, Cambridge University Press, 2012.

[55] J. T. Reis and W. K. Sauter, Phys. Rev. D **96**, 075031 (2017).

[56] J. Pumplin, D. R. Stump, J. Huston, H. L. Lai, P. M. Nadolsky and W. K. Tung, JHEP **0207**, 012 (2002).

[57] B. Acharya *et al.* (MoEDAL Collaboration), Phys. Lett. B **782**, 510 (2018).

[58] B. Acharya *et al.* (MoEDAL Collaboration), Phys. Rev. Lett. **118**, 061801 (2017).

[59] M. Benedikt, D. Schulte and F. Zimmermann, Phys. Rev. ST Accel. Beams **18**, 101002 (2015).

[60] I. K. Affleck and N. S. Manton, Nucl. Phys. B **194**, 38 (1982).

[61] O. Gould and A. Rajantie, Phys. Rev. Lett. **119**, 241601 (2017).

[62] O. Gould and A. Rajantie, Phys. Rev. D **96**, 076002 (2017).

[63] O. Gould, D. L. J. Ho and A. Rajantie, Phys. Rev. D **100**, no.1, 015041 (2019).

[64] V. Barone, *High-Energy Particle Diffraction*, Springer, 2002.

[65] B. R. Martin and G. Shaw, *Particle Physics* (Third Edition), John Wiley and Sons (2008).